2002

Optimal Recovery of Elastic Properties for Anisotropic Materials through Ultrasonic Measurements

Miao Sun

OPTIMAL RECOVERY OF ELASTIC PROPERTIES FOR ANISOTROPIC MATERIALS THROUGH ULTRASONIC MEASUREMENTS

By

Miao Sun

B.S. University of Shanghai for Science & Technology, 1989

A THESIS

Submitted in Partial Fulfillment of the

Requirements for the Degree of

Master of Science

(in Mechanical Engineering)

The Graduate School

The University of Maine

August, 2002

Advisory Committee:

Michael L. Peterson, Assistant Professor of Mechanical Engineering, Advisor

Donald A. Grant, R. C. Hill Professor and Chairman of Mechanical Engineering

Senthil Vel, Assistant Professor of Mechanical Engineering

OPTIMAL RECOVERY OF ELASTIC PROPERTIES FOR ANISOTROPIC MATERIALS THROUGH ULTRASONIC MEASURMENTS

By Miao Sun

Thesis Advisor: Dr. Michael L. Peterson

An Abstract of the Thesis Presented
in Partial Fulfillment of the Requirements for the
Degree of Master of Science
(in Mechanical Engineering)
August, 2002

Full knowledge of material elastic properties is required to facilitate design in many applications. The existence of misorientation between the geometric axes of the part and the material symmetry axes has in particularly created challenged in design of composite structure. In this thesis the potential for optimal identification of material symmetries for a general anisotropic material through a water immersion technique is explored. The concept is extensible to any class of symmetry groups and does not assume *a-priori* knowledge of the material. Initial experimental results for determining the elastic constants as well as locating the symmetry planes are presented. Many materials have not been investigated completely by a method such as the one described. The specific contribution of this work is to demonstrate this process for experimental data sets. The primary focus is on carbon-carbon composite material. The method is demonstrated using a single crystal with known properties.

ACKNOWLEDGEMENTS

This thesis is sponsored by the Ballistic Missile Defense Organization through the Office of Navel Research (ONR) Grant N00014-1-0519, Science Officer Dr. Y. D. S.

Special thanks are given to Dr. Cowin, S. C. and Dr. Mehrabadi, M. M. Dr. Cowin and Dr. Mehrabadi have shown continued activities in the area of identification of symmetry planes for a general anisotropic materials. They developed a theory of determining the normals to the symmetry planes, which frames the fundamentals of this thesis.

I would like to thank my advisor, Dr. Michael L. Peterson, for his guidance and understanding throughout this effort and for the tireless hours spent on the work. He is truly an exceptional professor, one who is not afraid to push students to reach their full potential.

I would like to thank Professor Donald Grant for all the readings and corrections on the papers. Without his input from his red pen, I would not have believed I could write a thesis. I also appreciate very much the support and guidance he has given me towards my degree and my further career choice. He truly is an inspiration to me

I would like to thank Dr. Senthil Vel for his help and time spent on this work. He helped me to look at the final results much differently than I would have had he not been a part of this thesis committee.

Thank you all.

TABLE OF CONTENTS

ACKNOWLEDGEMENTS ii

LIST OF TABLE vi

LIST OF FIGURES vii

LIST OF EQUATIONS viii

Chapter

1 INTRODUCTION 1

2 LITERATURE REVIEW 3

2.1 Method for the Determination of the Elastic Constants 3

2.2 Ultrasonic Transmission 4

2.3 Identification of Material Symmetry from the Measurements of Wave Velocity 6

3 THEORETICAL BACKGROUND 8

3.1 Elastic Constants 8

3.2 Anisotropic Media 10

3.3 Transformation Properties 13

3.4 Waves in Anisotropic Solids 16

3.5 Ultrasonic Immersion Technique for Determining the Elastic Constant for a General Anisotropic Solid 19

3.5.1 Introduction 19

3.5.2 Wave Velocity Measurement through Immersion Technique 20

3.5.3 Reconstruction of C_{ij} from Measured Phase Velocities 22

3.5.3.1 Fundamentals 22
3.5.3.2 Procedures for Optimization 23
3.5.3.3 Notes on Convergence and Error Issue on the Optimization Approach 25
4 ON STRUCTURE OF THE ELASTIC SYMMETRY OF AN ANISOTROPIC MATERIAL 27
4.1 Determination of Normals to the Symmetry Planes 27
4.2 Recovery of Principal Coordinate System 31
5 SIGNAL PROCESSING 36
5.1 Time Delay Estimation-Cross Correlation 36
5.2 Cross Correlation-Measure of Similarity 36
5.3 Relative Time Delay Estimation 37
6 EXPERIMENTAL SYSTEM 40
6.1 Experimental Setup 40
6.2 Experimental Measurements 41
6.3 Choice of Sample Material 43
7 RESULTS AND DISCUSSIONS 45
7.1 Results of Measured Phase Velocities 45
7.2 Results of Reconstructed Elastic Constants 47
7.3 Results of Estimation of Principal Coordinate System 48
7.4 Results with Carbon-Carbon Composites 52
8 CONCLUSIONS AND FUTURE WORK 57
REFERENCES 59

APPENDIX A. TENSOR CONVERSION FROM C_{IJKL} TO C_{IJ} 63

A. 1 Background 63

A. 2 Abbreviated Notations for σ_{ij}, ε_{ij}, and C_{ijkl} 64

A. 3 Transformations with Abbreviated subscripts 66

BIOGRAPHY OF THE AUTHOR 70

LIST OF TABLES

Table 7.1. Results of elastic constants and the associated Euler's angles with the carbon-carboncomposite material. 56

LIST OF FIGURES

Figure 3.1. Relation between axes and angles in conventional unit cell. 11

Figure 3.2 An illustration of 3D space lattices and some of crystal symmetry systems 12

Figure 3.3. Illustration of ultrasonic wave velocity measurement through a reference media (Top) and through an anisotropic sample with incident angle θ_i (Bottom). 20

Figure 3.4. Diagram of the coordinate system R=(x_1, x_2, x_3) and incident angle associated with the sample (Left). Wave propagation in the incident plane (x_1, φ_i) (Right). 22

Figure 4.1. Illustration of the unit normals to the symmetry planes. 30

Figure 4.2. Euler' angles. 32

Figure 4.3. An illustration of Euler's angles of an observation coordinate system R'' with respect to its principal coordinate system R^P. 35

Figure 5.1. Cross correlation. (a) signal x(n); (b) signal y(n) =x(n-4); (c) cross correlation r_{xy} between x(n) and y(n) 38

Figure 5.2. A plot of cross correlation 39

Figure 6.1. A schematic drawing of the experimental system for measuring elastic constants with immersion method. 40

Figure 6.2. A photograph of the experiment setup for measuring the elastic constants with the through-transmission technique. 41

Figure 7.1. An observation coordinate system R=(x_1, x_2, x_3) for ultrasonic measurement. 45

Figure 7.2. Phase velocity (in m/s) for an Al_2O_3 single crystal verse incident angle measured in (a) (x_1, 0^0), (b) (x_1, 45^0), (c) (x_1, 90^0), (d) (x_1, 135^0) incident planes. 46

Figure 7.3 (a). An illustration of normarls to the symmetry planes for a single crystal of aluminum oxide in an observation coordinate system R. (b). Location of the principal coordinate system R^p 50

Figure 7.4. An illustration of the miss-orientation between the geometric axes and the symmetric axes for a carbon-carbon composite. 54

LIST OF EQUITIONS

2.1.....5

3.1.....8

3.2.....8

3.3.....9

3.4.....10

3.5.....10

3.6.....13

3.7.....14

3.8.....14

3.9.....14

3.10.....14

3.11.....15

3.12.....15

3.13.....15

3.14.....16

3.15.....16

3.16.....16

3.17.....16

3.18.....17

3.19.....17

3.20.....17

3.21.....17

3.22....18
3.23....18
3.24....21
3.25....22
3.26....22
3.27....22
3.28....22
3.29....24
3.30....24
3.31....25
3.32....25
4.1....27
4.2....27
4.3....27
4.4....28
4.5....28
4.6....28
4.7....29
4.8....29
4.9....29
4.10....32
4.11....32
4.12....32

4.13.....33
4.14.....33
4.15.....33
4.16.....34
4.17.....34
5.1.....36
5.2.....37
5.3.....38
6.1.....42
6.2.....43
6.3.....43
7.1.....47
7.2.....47
7.3.....47
7.4.....48
7.5.....48
7.6.....48
7.7.....49
7.8.....51
7.9.....51
7.10.....52
7.11.....53
7.12.....54

A.1 63
A.2 63
A.3 63
A.4 63
A.5 64
A.6 64
A.7 65
A.8 65
A.9 65
A.10 66
A.11 66
A.12 66
A.13 67
A.14 67
A.15 67
A.16 68
A.17 68
A.18 68
A.19 68
A.20 68
A.21 68
A.22 69
A.23 69

1 INTRODUCTION

In a number of applications both the elastic and damping characteristics of the materials are required. Therefore, knowledge of the material properties is necessary to facilitate design of a composite structure. Even in cases where the planes of symmetry of the material are nominally well defined, significant variations of these planes can exist due to fiber misorientation of the principal material axes with respect to the geometrical axes. For the most part, misorientation is caused by material lay-up errors or warpage during manufacturing. In natural materials such as bone or wood, growth patterns may also cause the misorientation.

This thesis explores the mechanics associated with development of a water immersion technique for optimal recovery of elastic properties from ultrasonic measurements. Initial experimental results for determining the elastic constants and planes of symmetry are presented. Both single crystal and carbon-carbon composite materials are tested in this thesis. The single crystal used is a trigonal aluminum oxide with published elastic properties. For comparison, the samples of carbon-carbon composite are provided by Applied Thermal Sciences (Saco, ME) and produced by Fiber Materials, Inc. (Biddeford, ME). However, the concept is extensible to any class of symmetry groups and does not assume *a-priori* knowledge of the material symmetries.

In this technique, the phase velocity of an ultrasonic wave that is obliquely incident from a coupling liquid onto the test sample is determined. Water immersion is used in order to maintain good coupling between the sample and the ultrasonic transducers. Water immersion also makes it possible to generate the range of angles

required for the measurement. The elastic constants can be reconstructed from the velocity data by performing a Newton-Raphson nonlinear optimization to the experimental data as shown below.

A technique for the identification of elastic symmetries that the material possesses is also described in this thesis. From the knowledge of the symmetry properties, the principal axes with respect to its geometric axes are located. A method for determining the Euler's angles, which transfer the principal coordinate system to an observation coordinate system, is also presented in this work.

This introduction frames the thesis statement: the optimal recovery of elastic properties of a general anisotropic material is possible through use of an immersion ultrasonic technique. The specific contribution of this work is to demonstrate this process for an actual experimental data set. Extensive theoretical literature exists in this area, and for some special cases experimental results have been shown. However, this thesis develops a full sequence of work from measurement of the material properties to the definition of the three dimensional orientation of the material axes relative to the geometric axes.

2 LITERATURE REVIEW

2.1 Method for the Determination of the Elastic Constants

There are many methods used to measure the elastic constants of materials that are based on either the static or dynamic response of the material to an applied excitation [Schreiber et al., 1973]. The earliest method for the determination of the elastic constants was static testing, such as tensile, compressive, and torsional tests [Every and Schase, 2001]. Since the 1950s, an increasing need has arisen to know the elastic properties for anisotropic solids. Anisotropic materials are characterized by many more independent elastic constants. As a result of the testing needs, dynamic methods have been developed. The dynamic methods include ultrasonic transmission [Chimenti, 1997; Safaeinili et al., 1995], resonance method [Migliori et al., 1997] and light scattering. Compared to static methods, dynamic methods have many advantages. In most cases, dynamics methods are more accurate and are applicable to small samples. Dynamics methods also allow the study of viscoelasticity, dispersion and nonlinearities. However, the static methods require that multiple samples be used which requires more material and increases testing uncertainties in homogenous materials.

The most widely used methods are, or have been adapted from [Hellwege, 1979] :

1. Bulk acoustic and ultrasonic wave techniques, including the ultrasonic wave transmission and pulse superposition methods.
2. Resonance samples in the shape of rods, bars, parallelepipeds, plates, and more recently spheres.

3. Static deformation.

4. Light, neutron, and X-ray scattering, including Brillouin Scattering.

The accuracy of the methods is different, and the above list is approximately in order of decreasing accuracy [Hellwege, 1979]. The technique of ultrasonic transmission and Brillouin scattering are the most commonly used methods now [Hellwege, 1979]. Brillouin scattering allows the measurements to be made on very small samples. Samples that are less than a few millimeters are possible. However, Brillouin scattering can not provide any information about the effect of temperature on the elastic constants. The method of ultrasonic transmission holds significant advantages if a full set of elastic constants is required.

In this thesis the work focuses on techniques that use ultrasonic transmission for determining the elastic constants. Theoretical concepts are developed to allow the measurements to be understood.

2.2 Ultrasonic Transmission

The technique of using ultrasonic transmission to characterize material properties has developed significantly over the past fifteen to twenty years [Chimenti, 1997]. There are many references focusing on methods for obtaining the elastic constants using ultrasonic technique. Chimenti [1997] gave an overall review of the various methods available. A more general overview is given in a reference on elastic properties [Levy, et al, 2001].

Two primary techniques are used for ultrasonic transmission measurements. The immersion technique makes use of a sample immersed in liquid or in air [Safaeinili, 1995]. The second method is direct contact through transmission, where

the sample is in contact directly with the transducer [Buskirk and Cowin, 1986]. The immersion technique has been reported to have a number of advantages over the contact technique. Markham [1960], Papadakis et al. [1991]. Hosten, [1991], Rokhlin and Wang [1992] and others have stated that immersion methods are more straightforward to apply and usually give better results.

One of the primary disadvantages of the contact technique is that it requires cutting the sample in various directions. The thickness of the sample also needs to be larger than 5 cm [Every et al., 2001]. Other problems arise with contact methods when attenuation is measured. Attenuation is strongly influenced by the coupling agent between the transducers and the sample. In immersion techniques, the coupling fluid (water) is well behaved at all incidence angles and gives repeatable measurements as long as wetting of the sample is consistent. Even in more difficult cases, commercial surfactants are available to use in water-coupled systems.

Identification of elastic constants from the measurement of wave velocity using immersion techniques involves evaluating the Christoffel's equation

$$(C_{ijkl}\, n_l\, n_j - \delta_{ik} V^2 \rho) P_k = 0 \qquad 2.1$$

where C_{ijkl} are elastic constants to be determined, P_m is the polarization vector, V is the phase velocity of the ultrasonic wave, δ_{ik} is the Kronecker delta symbol, ρ is the mass density of the testing material, and n is the wave propagation direction with components of n_1, n_2, n_3.

Christoffel's equation is a cubic equation in the form of ρV^2 and applies to plane waves in both isotropic and anisotropic media. Two major approaches have

been applied to find the solution of the Christoffel's Equation. Numerical techniques have been extensively developed and can be found in many references [Aristegui and Baste, 1997 and 2000; Chu et al., 1994; Lee and Koc, 1989; Khathevich, 1962 and Neighbours et al., 1980]. Some of the available methods include the optimization method (Least-Squares minimization), principal invariants method [Khathevich, 1962] and iterative methods [Neighbours, 1980]. The other approach for solving the Christoffel's equation is the direct solution expressed in a closed form [Rokhlin, 1992; McSkimin, 1959 and 1961]. Use of the immersion technique is combined with an optimization approach for the determination of the elastic constants in this thesis.

2.3 Identification of Material Symmetry from the Measurements of Wave Velocity

Using either the immersion technique or the contact technique, the phase velocities measured at various directions in the material are not only used to determine elastic constants, they also contain information on the material symmetry. Knowledge of material symmetry is necessary for predicting its response to externally applied loads in some critical design applications. For example, coupled torsion and bending composite lay-ups are used in rotorcraft, and even in some simpler marine applications, where a specific misorientation of the symmetry axes relative to the geometric axes is required. Usually the symmetry axes and the geometric axes of the material are assumed to be coincident. However, misorientation between these two coordinate systems can exist in many cases [Sun and Peterson 2001; Aristegui and Baste, 1997]. Material lay-up in industrial composite manufacturing, growth processes such as annual rings in wood, and manufacturing warpage can lead to axis

misorientation. A general interest in the symmetry leads to the experimental determination of the material symmetry class explored in this thesis.

Many studies have concentrated on the methods of determining the material symmetry axes. Among them, Cowin, Mehrabadi and their co-workers have shown continued activities in this area.[1] Cowin first classified ten distinct material symmetries by number and the orientation of the symmetric plane or axes the material may posses [Cowin and Mehrabadi, 1987]. Locating the directions that are normal to these symmetric planes is equivalent to identification of the material symmetry. These directions must be a specific axis [Cowin, 1989] and a specific direction [Borgnis, 1955]. Upon knowing the elastic constants, a set of necessary and sufficient conditions for these directions to be normal to the symmetry plane was then established [Cowin, 1987, Cowin, 1989, Norris, 1988, and Norris, 1989].

Cowin's theory that is used for identification of the material symmetry does not consider the uncertainties associated with the elastic constants. Aristegui and Baste [1997] explicitly consider the uncertainties, but do not develop the idea of the symmetries. Another numerical technique is developed, double, namely the iterative numerical scheme, which use only the wave velocity measurements in an arbitrary coordinate system to find the material symmetry axes [Aristegui, 1997 and 2001]. Like all numerical techniques, the issue of stability and reliability of the numerical algorisms have become critical and have been intensively studied [Chu, 1994].

3 THEORETICAL BACKGROUND

The theoretical background is outlined here to support the mechanics of the experiments. From these concepts the measurements are understood and the symmetry concepts can be developed.

3.1 Elastic Constants

The infinitesimal strain tensor, ε_{ij}, describes the deformation in an acoustical excitation of a body. The strain is related to the particle displacement field u_{kl} through the stress-displacement equation

$$\varepsilon_{ij} = \frac{1}{2}(u_{i,j} + u_{j,i}) \qquad i,j = 1,2,3 \tag{3.1}$$

where $u_{i,j}$ and $u_{j,i}$ are the first partial derivative of displacement with respect to the coordinate index j and i, respectively. The summation convention has been employed.

By dynamics, the elastic restoring forces are defined in terms of stress field σ_{ij}. The equation of motion in a freely vibrating body is

$$\sigma_{ij,j} = \rho \ddot{u}_i \tag{3.2}$$

where $\sigma_{ij,j}$ is the partial derivative of stress with respect to coordinate index j. The superposed double dots, $\ddot{u}_i$ indicates the second partial derivative of displacement with respect to time.

The constitutive equation, Hooke's Law, states that the stress is linearly proportional to the strain as well as the converse. In general [Auld, 1997]

$$\sigma_{ij} = C_{ijkl}\varepsilon_{kl} \qquad 3.3$$

with the summation over the repeated subscripts k and l. The elements of the tensor C_{ijkl} in Equation 3.3 are called elastic constants. Conceptually, C_{ijkl} can also be referred to as "microscopic spring constants" [Auld, 1997]. The elastic constants are small for compliant materials and large for stiff materials.

Since there are nine equations in Equation 3.3 (corresponding to all combinations of the subscripts ij) and each contains nine strain terms, C_{ijkl} has indeed a total of 9^2=81 components [Frederick, 1965]. However, they are not all independent. The symmetry properties of the stress and strain

$$\sigma_{ij} = \sigma_{ji}, \varepsilon_{kl} = \varepsilon_{lk}$$

indicate

$$C_{ijkl} = C_{jikl} = C_{ijlk} = C_{jilk}$$

Thus, the independent components of C_{ijkl} are reduced from 81 to $6^2 = 36$. If Poynting's Theorem is applied [Nadeau, 1964], which shows

$$C_{ijkl} = C_{klij},$$

The number of independent constants are then further reduced to 21. This is the maximum number of independent elastic constants for any material symmetry. If the symmetry properties imposed by the microscopic nature of the material are considered, the number is typically less than 21. The number of independent constants has range from 2 (isotropic) to 21 (triclinic).

The four subscripts of C_{ijkl} can be simplified to two subscripts by using following the abbreviated subscript notation:

1	11
2	22
3	33
4	23 *or* 32
5	13 *or* 31
6	12 *or* 21

3.4

A [6×6] symmetric matrix form of C_{ij} is

$$\begin{bmatrix} C_{11} & C_{12} & C_{13} & C_{14} & C_{15} & C_{16} \\ & C_{22} & C_{23} & C_{24} & C_{25} & C_{26} \\ & & C_{33} & C_{34} & C_{35} & C_{36} \\ & & & C_{44} & C_{45} & C_{46} \\ & sym. & & & C_{55} & C_{56} \\ & & & & & C_{66} \end{bmatrix} \qquad 3.5$$

The simplification from C_{ijkl} to C_{ij} involves a tensor transformation from a fourth order three-dimensional tenor C_{ijkl} to a second order six-dimensional tensor C_{ijkl}. The conversion procedure strictly follows the tensor transformation law. Details of the transformation properties can be seen in Section 3.3. More details on the conversion procedures can be found in Appendix.

3.2 Anisotropic Media

It has been pointed out in the preceding section that the independent number of elastic constants C_{ij} can be reduced by considering symmetry properties of the material. A more mathematical explanation of this concept is that if the medium itself is symmetric with respect to a particular transformation of coordinates, then the stress and strain tensor must remain unchanged upon the same transformation. Therefore, the existence of the material's symmetry reduces the number of independent constants [Auld, 1990].

Unlike an isotropic media, where the properties are identical in all directions, an anisotropic media is more complicated. However, most anisotropic media do have some degree of symmetry. Before proceeding with wave propagation in anisotropic solid, a brief discussion of the symmetry classes for anisotropic media is provided.

In three dimensions, there are 32 symmetric point groups that can be subdivided into 14 space lattices [Musgrave, 1970]. These lattices are further grouped into seven crystal systems: triclinic, monoclinic, orthorhombic, tetragonal, cubic, trigonal, and hexagonal [Musgrave, 1970]. The first three symmetry classes (triclinic, monoclinic, orthorhombic) are considered to be the lower symmetry systems that the elastic bodies typically exhibit. The remaining is considered to be higher systems [Fedorov, 1968]. The derivation of the symmetry groups can be found in textbooks [Flint, 1952]. Figure 3.1 describes the relation between the axes and the angles of the unit cells in an anisotropic media. Some lower symmetry systems are given here to show how the symmetry properties reduce the number of independent elastic constants.

Triclinic. This is the absence of any material symmetry existing in the solid. There are no relationships between the 21 elastic constants, and none are zero.

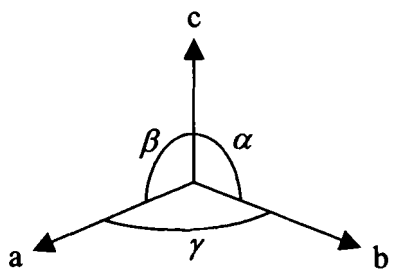

Figure 3.1. Relation between axes and angles in conventional unit cell.

Figure 3.2 (a) shows 3D space lattices in a triclinic crystal and the corresponding symmetry system. The angles α, β, γ are not equal and none of the angles are equal to 90^0 [Musgrave, 1970]. This result implies that no planes of symmetry exist in this system nor any rotational symmetry.

Monoclinic. A single mirror symmetry plane (a plane contains axis $\vec{a}$ and $\vec{c}$ in Figure 3.2 (b)) with a twofold rotational symmetry axis (axis $\vec{b}$) normal to it exists in a monoclinic crystal. Figure 3.2 (b) also shows that the angles $\alpha=\gamma=90^0$ and $\beta\neq 90^0$. The form of the elastic constant matrix for a monoclinic crystal is

$$\begin{bmatrix} C_{11} & C_{12} & C_{13} & 0 & C_{15} & 0 \\ & C_{22} & C_{23} & 0 & C_{25} & 0 \\ & & C_{33} & 0 & C_{35} & 0 \\ & & & C_{44} & 0 & C_{46} \\ & sym. & & & C_{55} & 0 \\ & & & & & C_{66} \end{bmatrix}$$

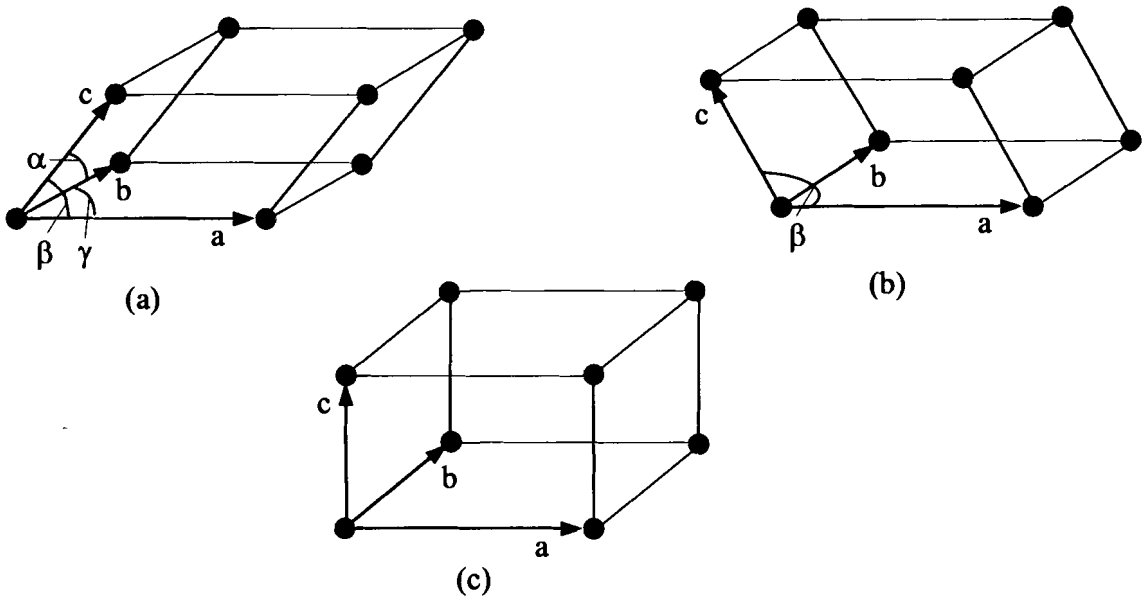

Figure 3.2. An illustration of 3D space lattices and some crystal symmetry systems. (a) triclinic ($\alpha\neq\beta\neq\gamma\neq 90^0$); (b) monoclinic (primitive, $\alpha=\gamma=90^0$, $\beta\neq 90^0$); (c) orthorhombic ($\alpha=\beta=\gamma=90^0$).

The corresponding Cartesian coordinate system is taken $\overrightarrow{x_2}$ to be the direction of $\vec{b}$ and $\overrightarrow{x_1}\,\overrightarrow{x_3}$ plane to be the symmetry plane. It is also applicable to set $\overrightarrow{x_3}$ parallel to $\vec{b}$, $\overrightarrow{x_1}\,\overrightarrow{x_2}$ to be the symmetry plane. In that case, $C_{15} = C_{25} = C_{35} = C_{46} = 0$, and $C_{16}, C_{26}, C_{36}, C_{45}$ are non-zero for a monoclinic material.

Orthorhombic. Orthorhombic symmetry is characterized by three mutually perpendicular mirror symmetry planes and twofold rotational symmetry axes perpendicular to these planes with angle $\alpha=\gamma=\beta=90^0$ as shown in Figure 3.2(c). A common convention for orienting the Cartesian coordinate system is $\overrightarrow{x_1}, \overrightarrow{x_2}, \overrightarrow{x_3}$ being the three perpendicular symmetry axes. Orthorhombic has nine elastic constants. In some contexts, orthorhombic is sometimes referred to as *orthotropic* symmetry, which is also commonly used in composite materials. The elastic constants for the orthorhombic case take the form.

$$\begin{bmatrix} C_{11} & C_{12} & C_{13} & 0 & 0 & 0 \\ & C_{22} & C_{23} & 0 & 0 & 0 \\ & & C_{33} & 0 & 0 & 0 \\ & & & C_{44} & 0 & 0 \\ & sym. & & & C_{55} & 0 \\ & & & & & C_{66} \end{bmatrix}$$

3.3 Transformation Properties

The elastic constants shown above are all given with respect to the corresponding crystal axes. However, this may not always be the circumstance faced in an engineering application. It may be more convenient to choose arbitrary axes for solving specific problems, or materials may be investigated where the uncertainty of

the symmetry properties exists. It is therefore necessary to consider how the elastic constants behave if transferred into other coordinate systems.

Since both stress (σ_{ij}) and strain (ε_{kl}) are second order three dimensional tensors, they all satisfy the tensor transformation laws, which are

$$\sigma_{mn}' = a_{mi} a_{nj} \sigma_{ij} \tag{3.6}$$

$$\varepsilon_{op}' = a_{ok} a_{pl} \varepsilon_{kl} \tag{3.7}$$

where $\sigma_{mn}', \varepsilon_{op}'$ are stress and strain tensors in the new coordinate system, respectively. a_{ij} is a [3×3] transformation matrix. The physical quantities of a_{ij} are direction cosines of the transformed coordinate axes with respect to its initial coordinate axes. The unit base vectors of the transformed coordinate system n_i' are related to the ones as the initial coordinate system n_i by

$$n_i' = a_{ij} n_j \tag{3.8}$$

Applying Equation 3.3 to Equation 3.6 gives

$$\sigma_{mn}' = C_{ijkl} a_{mi} a_{nj} \varepsilon_{kl} \tag{3.9}$$

Inversion of Equation 3.7 and substitution into Equation 3.9 gives

$$\varepsilon_{kl} = (a^{-1})_{ko} (a^{-1})_{lp} \varepsilon_{op}' = a_{ok} a_{pl} \varepsilon_{op}' \tag{3.10}$$

$$\sigma_{mn}' = C_{ijkl} a_{mi} a_{nj} a_{ok} a_{pl} \varepsilon_{op}' \tag{3.11}$$

Comparing Equation 3.11 with Equation 3.3 shows the elastic constants in the new coordinate system are

$$C'_{mnop} = a_{mi} a_{nj} a_{ok} a_{pl} C_{ijkl} \tag{3.12}$$

Satisfying the transformation formula (Equation 3.12) is sufficient for the elastic constants C_{ijkl} to be fourth order three-dimensional tensors.

It is important to perform coordinate transformations directly in an abbreviated subscript notation (six dimensional tensor C_{ij}) without the effort required to convert to full subscripts (three dimensional tensor C_{ijkl}), and reconvert back to the abbreviated notation after applying the transformation law, as shown in Section 3.1 (Equation 3.8). A very efficient technique for this purpose was developed by Bond [Bond, W. L. 1943]. Construction of the six dimensional tensor C_{ij} involves in the use of the symmetry properties of the stress and the strain. It also involves in construction of a [6×6] transformation matrices $[M]$, which is defined on the [3×3] transformation matrix [a]. [a] was introduced in the preceding section. [M] is defined by

$$[M]=\begin{bmatrix} a_{11}^2 & a_{12}^2 & a_{13}^2 & 2a_{12}a_{13} & 2a_{13}a_{11} & 2a_{11}a_{12} \\ a_{21}^2 & a_{22}^2 & a_{23}^2 & 2a_{22}a_{23} & 2a_{23}a_{21} & 2a_{21}a_{22} \\ a_{31}^2 & a_{32}^2 & a_{33}^2 & 2a_{32}a_{33} & 2a_{33}a_{31} & 2a_{31}a_{32} \\ a_{21}a_{31} & a_{22}a_{32} & a_{23}a_{33} & a_{22}a_{33}+a_{23}a_{32} & a_{21}a_{33}+a_{23}a_{31} & a_{22}a_{31}+a_{21}a_{32} \\ a_{31}a_{11} & a_{32}a_{12} & a_{33}a_{13} & a_{12}a_{33}+a_{13}a_{32} & a_{13}a_{31}+a_{11}a_{33} & a_{11}a_{32}+a_{12}a_{31} \\ a_{11}a_{21} & a_{12}a_{22} & a_{13}a_{23} & a_{12}a_{23}+a_{13}a_{22} & a_{13}a_{21}+a_{11}a_{23} & a_{11}a_{22}+a_{12}a_{21} \end{bmatrix} \quad 3.13$$

and

$$C'_{kl} = M_{ki}M_{lj}\,C_{ij} \quad 3.14$$

Equation 3.14 shows that C_{ij} is in fact a second order tensor since the tensor transformation law applies here. Details of the derivation of Equation 3.13 and 3.14 can be found in the Appendix.

The primary advantage of this method is that it can be applied directly to elastic constants given in abbreviated subscript notation as shown in the previous section (Section 3.2). Most importantly, unlike some constructions of the compliance tensor, for which tensor properties do not apply, the mathematical operations can be conveniently shown for all elements in a higher dimensional tensor. An example is furnished in Appendix to illustrate the features of this approach.

3.4 Waves in Anisotropic Solids

In the previous sections, the nature of material symmetry was considered. To discuss wave propagation in an anisotropic solid, the kinematic relations Equation 3.1 and equation of motion Equation 3. 2 should be revisited.

$$\varepsilon_{ij} = \frac{1}{2}(u_{i,j} + u_{j,i}) \qquad 3.15\ (3.1)$$

$$\sigma_{ij,j} = \rho \ddot{u}_i \qquad 3.16\ (3.2)$$

The constitutive Equation 3.3 are substituted into Equation 3.15 and 3.15 to obtain

$$C_{ijkl} u_{k,jl} = \rho \ddot{u}_i \qquad 3.17$$

where $u_{k,jl}$ is the second partial derivative of displacement with respect to coordinate index j and l. Double dot, $\ddot{u}_i$ indicates the second derivative of displacement with respect to time and ρ is the density of the material.

A plane wave solution to this second order differential equation is assumed to be of the form

$$u_k = A_k p_k e^{i(Kx - \omega t)} \qquad 3.18$$

where A_k are components of the displacement amplitude; p_k are unit displacement polarization vectors traveling in the directions determined by the relationship between the incident angles and the material symmetry axes; $K = \omega/c$ is the wave number with wave speed in the solid c and frequency ω [Auld, 1997].

Substituting Equation 3.18 into Equation 3.17 gives an eigenvalue equation (Christoffel's Equation), then,

$$(C_{ijkl} n_j n_l - \delta_{ik} \rho V^2) p_k = 0 \tag{3.19}$$

This is a cubic polynomial in ρV^2, where V is the phase velocity of the ultrasonic wave, δ_{ik} is the Kronecker delta symbol, n is a unit vector in the direction of wave propagation with components of n_1, n_2, n_3. Equation 3.19 can be rewritten in matrix form:

$$\begin{bmatrix} \Gamma_{11} - \rho V^2 & \Gamma_{12} & \Gamma_{13} \\ & \Gamma_{22} - \rho V^2 & \Gamma_{23} \\ sym. & & \Gamma_{33} - \rho V^2 \end{bmatrix} \begin{Bmatrix} p_1 \\ p_2 \\ p_3 \end{Bmatrix} = 0 \tag{3.20}$$

where

$$\Gamma_{ik} = C_{ijkl} n_l n_j \tag{3.21}$$

is referred to as the Christoffel's tensor.

Christoffel's tensor is indeed a second order tensor, subject to the symmetry condition $\Gamma_{ik}=\Gamma_{ki}$ [Hearmon, 1961]. Therefore, six independent components of the Christoffel's tensor exist. Expansion of Equation 3.21 following indicial rules

gives

$$\Gamma_{11} = n_1^2 C_{11} + n_2^2 C_{66} + n_3^2 C_{55} + 2n_2 n_3 C_{56} + 2n_3 n_1 C_{15} + 2n_1 n_2 C_{16}$$
$$\Gamma_{22} = n_1^2 C_{66} + n_2^2 C_{22} + n_3^2 C_{44} + 2n_2 n_3 C_{24} + 2n_3 n_1 C_{46} + 2n_1 n_2 C_{26}$$
$$\Gamma_{33} = n_1^2 C_{55} + n_2^2 C_{44} + n_3^2 C_{33} + 2n_2 n_3 C_{34} + 2n_3 n_1 C_{35} + 2n_1 n_2 C_{45}$$
$$\Gamma_{12} = n_1^2 C_{16} + n_2^2 C_{26} + n_3^2 C_{45} + n_2 n_3 (C_{25} + C_{46}) + n_3 n_1 (C_{14} + C_{56}) + n_1 n_2 (C_{12} + C_{66})$$
$$\Gamma_{13} = n_1^2 C_{15} + n_2^2 C_{46} + n_3^2 C_{35} + n_2 n_3 (C_{36} + C_{45}) + n_3 n_1 (C_{13} + C_{55}) + n_1 n_2 (C_{14} + C_{56})$$
$$\Gamma_{23} = n_1^2 C_{56} + n_2^2 C_{24} + n_3^2 C_{34} + n_2 n_3 (C_{44} + C_{23}) + n_3 n_1 (C_{36} + C_{45}) + n_1 n_2 (C_{25} + C_{46})$$

3.22

In order to have a nontrivial solution of the Chirstoffel's equation, the determinant of the coefficient matrix of Equation 3.20 must vanish [Musgrave, 1970].

$$\left| \Gamma_{ij} - \delta_{ij} \rho V^2 \right| = 0 \qquad 3.23$$

Since the Christoffel's tensor Γ_{ik} is symmetric, its eigenvalues ρV^2 are real and the eigenvectors p_k are mutually orthogonal. Therefore, for any given direction **n**, three modes can be generated with different velocities and polarizations. For the principal propagation directions, pure propagation modes can be generated: one longitudinal wave when **P**=**n**, and two transverse waves when **P**×**n**=0. In general, a quasi-longitudinal wave (QL) and two quasi-transverse waves (QT1 and QT2) are excited. The phase velocities corresponding to each of these wave modes are known to be functions of the elastic properties of the material [Musgrave, 1970].

3.5 Ultrasonic Immersion Technique for Determining the Elastic Constant for a General Anisotropic Solid

3.5.1 Introduction

From the preceding section, the phase velocities of the ultrasonic wave are related to the elastic constants of the sample through the Christoffel's equation (Equation 3.19). Also, as mentioned in the previous chapter, wave velocity measurement using an immersion technique is an ideal method for determining the elastic constants of a general anisotropic material. The general concept of this technique is to measure the phase velocities of the ultrasonic wave that is obliquely incident from liquid onto the testing sample. Water is used as the immersion media in order to have good coupling between the sample and the ultrasonic transducers [Hosten, 2001].

From the velocity data the elastic constants can be reconstructed by using an inverse technique [Hosten, 2001]. Practically speaking, there is more data than the independent elastic constants [Every, 1992]. Therefore, this is an over-determined problem, which leads to the use of a nonlinear Newton-Raphson optimization approach to find a set of elastic constants. In this thesis, a basic optimization is adopted by minimizing the square of Equation 3.23 so as to obtain the set of elastic constants.

To obtain accurate phase velocities of the waves, cross-correlation is used to measure the relative time delay between the reference signal propagating in the water only and the signal that results from the propagation through the sample [Peterson, 1997, Hosten, 2001].

3.5.2 Wave Velocity Measurement through Immersion Technique

The ultrasonic wave, typically an ultrasonic pulse in most experimental work, is generated by an electronic pulser, which excites a piezoelectric transducer, propagates through the water and the testing sample. The signal is received by another piezoelectric transducer (Figure 3.3), then is amplified and acquired digitally. The transducers and the sample are all immersed in the water, the coupling media. For the convenience of measurement a coordinate system $R = (x_1, x_2, x_3)$ is chosen in such a way that the origin of R is set at the center of the sample. Unit base vector $\mathbf{x_1}$ is normal to the interface, unit base vectors $\mathbf{x_2}$ and $\mathbf{x_3}$ follow the right hand rule.

In general, for a fluid coupling of an ultrasonic wave into an anisotropic plate, and for an arbitrary incident angle θ, three modes of the wave are excited. A quasi-longitudinal wave (QL), a slow quasi-transverse wave (QT1) and a fast quasi-transverse wave (QT2) are generated in the solid (Figure 3.3). These waves propagate at different phase velocities and their velocity vectors all lie in the incident plane (a

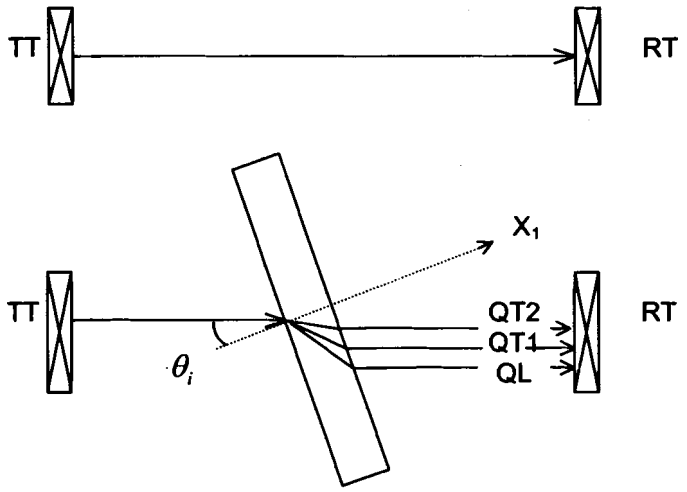

Figure 3.3. Illustration of ultrasonic wave velocity measurement through a reference media (Top) and through an anisotropic sample with incident angle θ_i (Bottom).

plane consisting axis $\mathbf{x}_1$ and the incident wave). If this plane coincides with a plane of the material symmetry, only one transverse wave and one longitudinal wave are generated [Auld, 1990].

To measure the phase velocity, the length of the wave path through the plate must be known. The relative time delay τ_i between the transmitted signal through the sample and the time through a known media must also be obtained. In this case the known media is the water path without the sample. The time delay is obtained by cross correlation [Peterson, 1997]. The length of the wave path is obtained by Snell-Descartes Law [Auld, 1990]. The velocities then can be calculated by the formula [Hosten, 2001]:

$$V_i(x_1,\varphi)=\frac{V_0}{\sqrt{1+\frac{V_0\tau_i}{d}\left(\frac{V_0\tau_i}{d}-2\cos\theta_i\right)}} \qquad 3.24$$

where V_0 is the wave velocity in the water, τ_i is time delay, θ_i is the incident angle, d is the thickness of the sample, and $(\mathbf{x}_1, \varphi)$ indicts the wave incident plane.

For identifying the elastic constants of a general anisotropic material, experimental data is collected from four incident planes ($\mathbf{x}_1$, φ), where $\varphi=0^0$, 45^0, 90^0 and 135^0 are called the azimuthal angles [Aristegui, 1990]. This procedure can also be explained by saying the testing plate is rotated through a certain angle ($\varphi=0^0$, 45^0, 90^0 and 135^0) with respect to the $\mathbf{x}_1$ axis.

An illustration of the geometric coordinate system R and the incident planes is given in Figure 3.4.

3.5.3 Reconstruction of C_{ij} from Measured Phase Velocities

3.5.3.1 Fundamentals

The elastic constants can be reconstructed if a large number of wave velocity data points are available by performing a Newton-Raphson nonlinear optimization. The secular equation, Equation 3.21, for the optimization is

$$\left|\Gamma_{ij} - \delta_{ij}\rho V^2\right| = 0 \qquad 3.25$$

In the general case, three phase velocities corresponding to the three wave modes are three solutions of this non-linear cubic equation. Due to experimental errors, every measured phase velocity V is approximately the solution of Equation 3.25

$$f(V_{\exp}, C_{ij}) = \left|\Gamma_{ij} - \delta_{ij}\rho V^2\right| \cong 0 \qquad 3.26$$

where $f(V_{\exp}, C_{ij})$ is the left hand side of Equation 3.25 and $V_{\exp}(n)$ indicates the phase velocities measured from the four incident planes described in section 3.5.2.

Reconstruction of all the twenty-one components of C_{ij} can be performed by

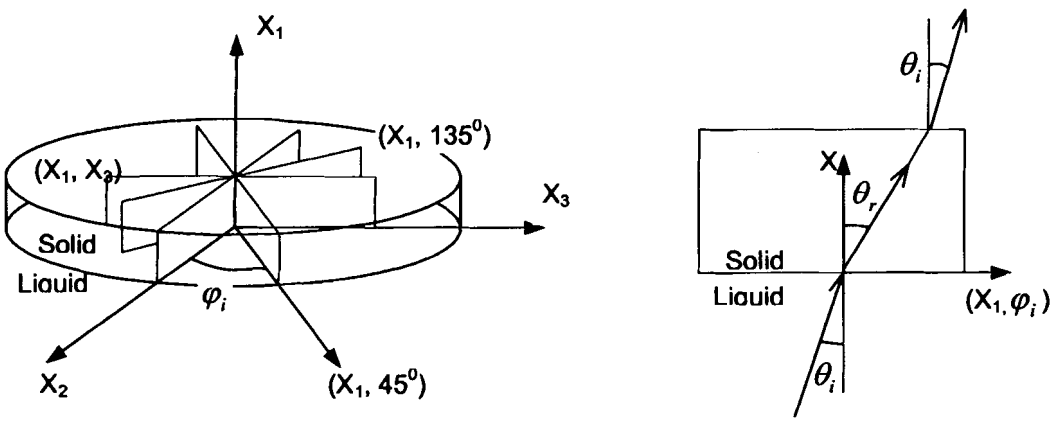

Figure 3.4. Diagram of the coordinate system R=(x_1, x_2, x_3) and incident angle associated with the sample (Left). Wave propagation in the incident plane (x_1, φ_i) (Right).

minimizing an objective function $F(C_{ij})$, which is the sum of squares of the secular Equation 3.26.

$$C_{ij} = \min\{F(C_{ij})\} \tag{3.27}$$

with

$$F(C_{ij}) = \sum_{i=1}^{n}[f(V_{\exp}(i), C_{ij})]^2 \tag{3.28}$$

where n =all data points collected from the four incident planes.

Equation 3.28 shows that the method minimizes the effect of random deviations of experimental data on the results of reconstruction. The wave velocity measurements are indeed embodied in each objective function to be minimized. There are more experimental data points than the number of the independent elastic constants. Therefore Equation 3.26 is constructed from an over-determined system of the functions $f(V_{\exp}, C_{ij})$ [Every, 1990]. Contrary to another method [Rokhin et al., 1992] that considers the direct solutions of Christoffel's Equation (Equation 3.19), this minimization problem requires no mode distinction [Aristegui and Baste et al., 1997]. This is simply because each of the modes generated is the solution of Christoeffl's Equation and should satisfy Equation 3.25. For the general case, the velocity data are collected from four incident planes ($\mathbf{x}_1$, 0^0), ($\mathbf{x}_1$, 45^0), ($\mathbf{x}_1$, 90^0), and ($\mathbf{x}_1$, 135^0) associated with various incident angles.

3.5.3.2 Procedures for Optimization

In this thesis, the minimization was performed by using a standard MATLAB optimization function, which is based on the Newton-Raphson method described above. A successful implementation of optimization requires reasonable estimates of

the elastic constants as initial values to feed into the algorithm. In this work, a single crystal of aluminum oxide was used to test both the analysis and measurement work. The initial elastic constants for the algorithm were obtained from a material handbook [Hellwege, 1979].

The procedures of the optimization for reconstruction of the elastic constants C_{ij} used in this thesis are as follows:

(1). A set of phase velocities $V_{exp}(1),...V_{exp}(n)$, which correspond to each of these wave modes, is measured from four incident planes. Twenty-five different incident angles are needed at each of the four incidental planes to make up a total of 100 data points.

(2). Using a trial set of elastic constants C^0_{ij} as an initial guess to construct a $f^0(V_{exp}, C^0_{ij})$, and an objective function $F^0(C_{ij})$ to be minimized through Equation 3.26 and Equation 3.28, Γ^0_{ij} can be obtained using Equation 3.8.

(3). At each step (kth) of the iteration, an error e_k, which is defined as the difference between the C_{ij}^k and the desired C_{ij}, will result. The closer the C_{ij}^k are to the C_{ij}, the smaller, on the average, the error will be.

(4). This procedure may be iterated until

$$e_k - e_{k-1} = C_{ij}^{(k)} - C_{ij}^{(k-1)} \leq \varepsilon \qquad 3.29$$

where ε is a pre-assigned tolerance of a very small quantity [Pierre, 1969]. In this thesis, $\varepsilon=10^{-4}$, for the test case.

3.5.3.3 Notes on Convergence and Error Issue on the Optimization Approach

The Newton-Raphson formula for finding roots of an equation

$$f(V, C_{ij}) = 0$$

is given by [Kunz, 1957]

$$C_{ij}^{(k+1)} = C_{ij}^{(k)} - \frac{f(C_{ij}^{(k)})}{f(C_{ij}^{(k+1)})} \qquad 3.30$$

To determine the convergence of iteration in the Newton-Raphson method, a Taylor's series is used to expand $f(C_{ij})$ at one of the iterations C_{ij}^{k}.

$$f(C_{ij}) = f(C_{ij}^{k}) + (C_{ij} - C_{ij}^{k}) f'(C_{ij}^{k}) + \frac{1}{2}(C_{ij} - C_{ij}^{k})^2 f''(\xi) + \ldots \qquad 3.31$$

By using Equation 3.29 and Equation 3.30, Equation 3.31 turns into [Kunz, 1957]

$$e_{k+1} = e_k^{\,2} \frac{f''(\xi)}{2f'(C_{ij}^{k})} \qquad 3.32$$

A general rule for convergence of this method is given by Kunz (1957). If the absolute value of $\frac{f''(\xi)}{2f'(C_{ij}^{k})}$, for any C_{ij}^{k} in an upper bound region, is small enough in the neighborhood of the root C_{ij}, and if the C_{ij}^{k} is known to approximate the C_{ij}, then C_{ij}^{k+1} approximate the C_{ij} , therefore, the (k+1)th iteration converges.

The quality of this optimization approach depends on the quality of the first approximation and the rapidity of convergence of the procedure. There is no guarantee that a given procedure will converge, or that it will converge to the desired solution [Meyer, 1975]. It sometimes happens that a given procedure may converge

to a local minimum that is not the absolute minimum sought. This can be checked by starting at a different set of initial guess to check if it ends up with the same minimum [Meyer, 1975].

With the immersion method, the procedure of identification of C_{ij} can reache errors at as low as a few percentage points level. A statistical error analysis may also be more appropriate for approaching realistic values [Hoston, 2001].

4 ON STRUCTURE OF THE ELASTIC SYMMETRY OF AN ANISOTROPIC MATERIAL

4.1 Determination of Normals to the Symmetry Planes

Based on knowledge of the elastic constants C_{ijkl} of an anistropic material, identification of elastic symmetry possessed by the material was developed by Cowin (1987, 1989) and Norris (1988). Two tensors A_{ij} (Voigt tensor) and B_{ij} (dilatational modulus) are required to determine the elastic symmetry planes of the material. These tensors are defined by:

$$A_{ij} = C_{ijkk}, \quad B_{ij} = C_{ikjk} \tag{4.1}$$

If the abbreviated subscript notation C_{ij} is used through the C_{ijkl} (Section 3.5.3.1), by applying the indicial notation, tensors A (Voigt tensor) and B (dilatational modulus) can be expressed in terms of the components of C_{ij}

$$A = \begin{bmatrix} C_{11}+C_{12}+C_{13} & C_{16}+C_{26}+C_{36} & C_{15}+C_{25}+C_{35} \\ C_{16}+C_{26}+C_{36} & C_{12}+C_{22}+C_{23} & C_{14}+C_{24}+C_{34} \\ C_{15}+C_{25}+C_{35} & C_{14}+C_{24}+C_{34} & C_{13}+C_{23}+C_{33} \end{bmatrix} \tag{4.2}$$

$$B = \begin{bmatrix} C_{11}+C_{55}+C_{66} & C_{16}+C_{26}+C_{45} & C_{15}+C_{46}+C_{35} \\ C_{16}+C_{26}+C_{45} & C_{22}+C_{44}+C_{66} & C_{24}+C_{34}+C_{56} \\ C_{15}+C_{46}+C_{35} & C_{24}+C_{34}+C_{56} & C_{33}+C_{44}+C_{55} \end{bmatrix} \tag{4.3}$$

A vector is normal to a symmetry plane of a linear elastic material if and only if the vector is an eigenvector of tensor A and B respectively. These normals are in a specific direction and define a specific axis by Cowin's theory of (1989). Once the specific directions and specific axes are obtained by solving the eigenvector problem of A and B, the elastic symmetry of the anisotropic material can be determined.

An example is given here to demonstrate the procedure. A set of elastic constants of a carbon-carbon composite material is used. The values of the elastic constants (in GPa) were obtained from our initial work [Sun, M. and Peterson, M. 2001], where a contact technique [Buskirk et al, 1986] was applied for ultrasonic measurement.

$$[C]=\begin{bmatrix} 47.601 & 44.371 & 46.342 & 0 & 0 & 0 \\ & 18.906 & 20.327 & 0 & 0 & 0 \\ & & 18.839 & 0 & 0 & 0 \\ & & & 3.1112 & 0 & 0 \\ & \text{sym.} & & & 5.2180 & 0 \\ & & & & & 4.5369 \end{bmatrix} GPa \qquad 4.4$$

With a rotation through 30^0 about the x_3 coordinate axis, a new set of elastic constants that are not in its principal coordinate system were determined using Equation 3.13. The rotation is taken as counterclockwise as one looks to the origin O along the axis of rotation [Shame, 1966]. The transformation matrix [a], with respect to the fixed coordinate system R, is

$$[a]=\begin{bmatrix} \cos(30^0) & \sin(30^0) & 0 \\ -\sin(30^0) & \cos(30^0) & 0 \\ 0 & 0 & 1 \end{bmatrix} \qquad 4.5$$

A [6×6] Bond transformation matrix [M] was defined by Equation 3.14 (see section 3.3). Thus,

$$C'=M*C*M^{-1}=\begin{bmatrix} 47.999 & 36.799 & 39.838 & 0 & 0 & -1.8413 \\ & 33.651 & 26.831 & 0 & 0 & -1.0584 \\ & & 18.839 & 0 & 0 & -1.1265 \\ & & & 3.6379 & -0.9123 & 0 \\ & \text{sym.} & & & 4.6913 & 0 \\ & & & & & -3.0346 \end{bmatrix} GPa$$

4.6

where C' are the transformed elastic constants in the rotated coordinate frame.

Tensor A and B as defined in Equation 4.1 were found. These tensors are then used to obtain the unit normals to the planes of symmetry.

$$A = \begin{bmatrix} 124.63 & -23.690 & 0.000 \\ 23.690 & 97.281 & 0.000 \\ 0 & 0 & 85.508 \end{bmatrix}$$
$$B = \begin{bmatrix} 49.656 & -13.337 & 0.000 \\ 13.337 & 34.254 & 27.168 \\ 0 & 27.168 & 0.000 \end{bmatrix} \qquad 4.7$$

Eigenvectors of A and B are:

$$[Vec\_A] = \begin{bmatrix} -0.500 & 0 & -0.866 \\ -0.866 & 0 & 0.500 \\ 0 & 1 & 0 \end{bmatrix}$$
$$[Vec\_B] = \begin{bmatrix} -0.500 & 0 & -0.866 \\ -0.866 & 0 & 0.500 \\ 0 & 1 & 0 \end{bmatrix} \qquad 4.8$$

Equation 4.8 shows that all three pairs of eigenvectors of the A and B are coincident. Therefore, all three eigenvectors are unit vectors to the planes of symmetry that were assumed in the original elastic constant set (Equation 4.4). These three eigenvectors are

$$\begin{aligned} e_1 &= -0.5n_1 - 0.866n_2 + 0n_3 \\ e_2 &= 0n_1 + 0n_2 + n_3 \\ e_3 &= -0.866n_1 + 0.5n_2 + 0n_3 \end{aligned} \qquad 4.9$$

where n_k are unit base vectors of the coordinate system. Figure 4.1 illustrates the locations of the symmetry planes and the corresponding normals to the symmetry planes.

Theoretically, for an orthotropic material, the three eigenvectors of tensor A and B are coincident and are aligned with their crystallographic directions [Cowin, 1987]. For a monoclinic media, only one pair of eigenvector is identical. In the case where none of the eigenvectors is in common indicates that the material tested possesses triclinic symmetry.

However, due to the experimental errors in the measurements, the eigenvectors of A and B do not exactly line up. Since the eigenvectors of A and B are orthogonal eigenvectors, respectively, a normal to the symmetry plane is contained in an angle around the average directions between the closest eigenvectors of A and B [Aristegui, 2000]. The closest eigenvectors of A and B can be determined by investigating the angular deviation between each pair of eigenvectors. In general the eigenvector pair that exhibits the small angular deviation is considered to be a good estimate of a normal to a symmetry plane [Aristegui, 2000]. A detailed procedure for determining the orientation of a normal to a symmetry plane is in Section 7.3.

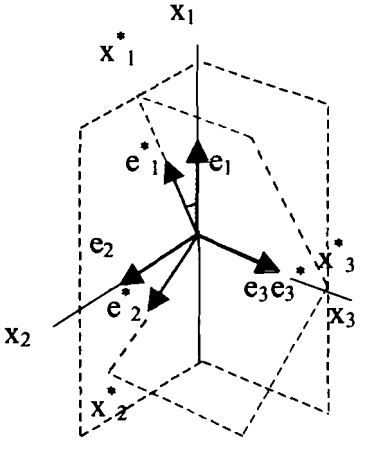

Figure 4.1. Illustration of unit normals to the symmetry planes. e_1, e_2 and e_3 are the normal to the symmetry plane without rotation. e_1^*, e_2^*, and e_3^* indicate the case of rotation of 30^0 with respect to x_3.

4.2 Recovery of Principal Coordinate System

Once the normals to the symmetry planes are known, recovery of the principal coordinate system becomes relevant. In some design applications, knowledge of the principal coordinate system is necessary to predict the misorientation between the symmetry axes and the geometric axes within the material. It can also increase the understanding of the warpage and coupled deformation.

As described in section 3.2, seven symmetrical crystal systems exist. Each system is characterized by the number of symmetry planes it possesses and the orientations of these symmetry planes. The orientation of a principal coordinate frame R^P with respect to an observation coordinate system R can be specified by a set of Euler's angles $\delta = (\alpha, \beta, \gamma)$. Recalling Section 3.3 gives that the Euler's angles indeed relate the two coordinate systems R^P and R through a set of successive rotations between the two systems.

No general agreement on the notation of Euler's angles exists, but one of the most common, namely, α, β, and γ, in sequence, is shown in Figure 4.2. The initial coordinate system R with a set of Cartesian axes $\mathbf{x}_1$, $\mathbf{x}_2$, $\mathbf{x}_3$ is first rotated through an angle α about the x_3 axis. A further rotation through angle β about the *transformed* $\mathbf{x}_1$ brings the body into a coordinate system R'. Finally a rotation γ about the *transformed* x_3 put the system into a coordinate system R^P with a set of Cartesian axes $\mathbf{x}_1^P$, $\mathbf{x}_2^P$, and $\mathbf{x}_3^P$. The rotations are performed as counterclockwise as one looks to the origin **O** along the axis of rotation [Shame, 1966]. It is also important to recall that the orientation of the rotated coordinate frame is dependant on the order of the rotations.

Transformations from the initial R to the coordinate system R^P may also be obtained through three-transformation matrix $a(\alpha)$, $a(\beta)$, $a(\gamma)$ as shown in Section 3.3.

$$\{x_i^P\} = [a(\alpha)][a(\beta)][a(\gamma)]\{x_i\} = [M]\{x_i\} \tag{4.10}$$

where

$$[a(\alpha)] = \begin{bmatrix} \cos(\alpha) & \sin(\alpha) & 0 \\ -\sin(\alpha) & \cos(\alpha) & 0 \\ 0 & 0 & 1 \end{bmatrix}$$

$$[a(\beta)] = \begin{bmatrix} 1 & 0 & 0 \\ 0 & \cos(\beta) & \sin(\beta) \\ 0 & -\sin(\beta) & \cos(\beta) \end{bmatrix} \tag{4.11}$$

$$[a(\gamma)] = \begin{bmatrix} \cos(\gamma) & \sin(\gamma) & 0 \\ -\sin(\gamma) & \cos(\gamma) & 0 \\ 0 & 0 & 1 \end{bmatrix}$$

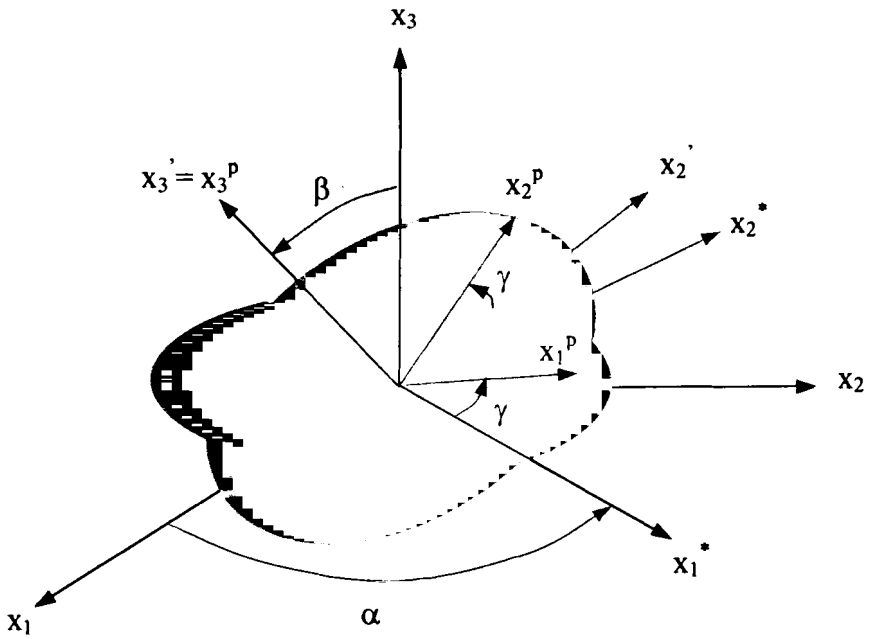

Figure 4.2. Euler's angles.

and

$$[M]=\begin{bmatrix} c\alpha\, c\gamma - s\alpha\, c\beta\, s\gamma & s\alpha\, c\gamma + c\alpha\, c\beta\, s\gamma & s\beta\, s\gamma \\ -c\alpha\, s\gamma - s\alpha\, c\beta\, c\gamma & -s\alpha\, s\gamma + c\alpha\, c\beta\, c\gamma & s\beta\, c\gamma \\ s\alpha\, s\beta & -c\alpha\, s\beta & c\beta \end{bmatrix} \qquad 4.12$$

$$c = \cos;\ s = \sin$$

Locating the principal coordinate system R^P (if it exists within the material) is equivalent to the determination of the set of angular unknowns, $\delta=(\alpha, \beta, \gamma)$. Each of the angular unknowns corresponds to a normal to the symmetry plane and transforms the coordinate system from R^P to R. In general, two rotations of the coordinate system are enough to characterize the orientation of the principal coordinate system R^P [Auld, 1990. Aristegui, 2000]. In other words, any principal coordinate system R^P, with respect to the observation coordinate system R, can be characterized by a set of angular unknowns with at least one of these unknowns being equal to zero. Therefore the transformation matrix [M] in Equation 4.12, if $\gamma=0$ as in this thesis, can be reduced to

$$[M]=\begin{bmatrix} \cos(\alpha) & \sin(\alpha) & 0 \\ -\sin(\alpha)\cos(\beta) & \cos(\alpha)\cos(\beta) & \sin(\beta) \\ \sin(\alpha)\sin(\beta) & -\cos(\alpha)\sin(\beta) & \cos(\beta) \end{bmatrix} \qquad 4.13$$

To demonstrate the procedure of determining the Euler's angles of a principal coordinate system with respect to the observation coordinate system, the example given in the preceding section, is considered again. Following a counterclockwise rotation through 30^0 (α) about the $\mathbf{x}_3$ axis as it was introduced in section 4.1, a counterclockwise rotation through 10^0 (β) about the transferred $\mathbf{x}_1$ is performed

(Figure 4.3) to obtain the elastic constant C'' in a transferred coordinate system R''. In this case γ=0.

$$C''= M'C'(M')^{-1}$$

$$= \begin{bmatrix} 47.999 & 36.891 & 39.747 & 0.520 & 0.320 & -1.813 \\ & 33.665 & 26.371 & -0.003 & 1.534 & -10.498 \\ & & 19.745 & -2.530 & 2.260 & -11.019 \\ & & & 3.178 & -0.824 & -0.264 \\ & \text{sym.} & & & 4.459 & 1.321 \\ & & & & & -2.802 \end{bmatrix} GPa \qquad 4.14$$

Normals to the symmetry planes (eigenvectors of tensors A and B) with respect to the transformed coordinate frame R'' are obtained (see section 4.1)

$$\begin{aligned} e_1'' &= 0.5\, n_1'' + 0.8529\, n_2'' - 0.1504\, n_3'' \\ e_2'' &= 0\, n_1'' + 0.1736\, n_2'' + 0.9848\, n_3'' \\ e_3'' &= 0.866\, n_1'' - 0.4924\, n_2'' + 0.0868\, n_3'' \end{aligned} \qquad 4.15$$

where n_1'', n_2'', n_3'' are the unit base vectors of the coordinate system R''.

Since any of the eigenvectors in 3.11 is a normal to the symmetry plane, the Euler's angles δ=(α, β, 0) can be extracted from any one of the three components of the eigenvectors in Equation 3.11.

$$\begin{aligned} e_3'' &= 0.866\, n_1'' - 0.4924\, n_2'' + 0.0868\, n_3'' \\ &= \cos(\alpha)\, n_1'' - \sin(\alpha)\cos(\beta)\, n_2'' + \sin(\alpha)\sin(\beta)\, n_3'' \end{aligned} \qquad 4.16$$

Therefore

$$\begin{aligned} \alpha &= 30^0 \\ \beta &= 10^0 \\ \gamma &= 0 \end{aligned} \qquad 4.17$$

Figure 4.3 illustrates the Euler's angles of a non-principal observation coordinate system R'' with respect to its principal coordinate system R^P in a carbon-carbon composite.

For the case where the material possess higher symmetries (tetragonal, hexagonal or isotropic, see Section 3.2), the principal coordinate system can be identified, based on the symmetry model assumed. The orientation of the axes is found by investigating the deviation between the elastic constants reconstructed in R^P and the one satisfying the chosen symmetry model [Aristegui, 1997]. In the case where the material possesses only a single symmetry plane, identification of the symmetry is reduced to finding one unknown of the Euler's angles with the two other angles zero. On the other hand, if no symmetry can be determined by section 4.1, three Euler angles $\delta=(\alpha, \beta, \gamma)$ are necessary to search for R^P [Aristegui, 1997].

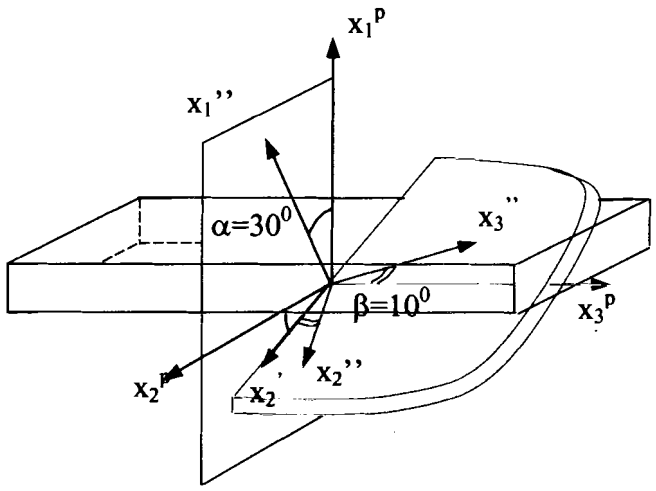

Figure 4.3. An illustration of Euler's angles of an observation coordinate system R'' with respect to its principal coordinate system R^P. R'' is obtained from R^P by two rotations $\alpha=30^0$ and $\beta=10^0$.

5 SIGNAL PROCESSING

To obtain accurate relative time delays, the cross-correlation was used [Peterson, 1997]. Cross-correlation algorithms were used to estimate the transmit time difference (τ) between two signals. In this thesis an ultrasonic waveform transmitted through water (the reference signal) is compared to a signal through an unknown sample. The sample used in this set up is a single crystal of aluminum oxide.

5.1 Time Delay Estimation-Cross Correlation

Cross correlation is a mathematical operation that is to measure the similarity of two waveforms [Proakis, et. al, 1997]. It is widely used to estimate the relative time between two signals. Therefore, in radar, digital communications and other areas in science and engineering, cross correlation has broad applications [Proakis, et. al, 1997]. The basic concept of the cross correlation is discussed as well as its relationship to time delay estimation problem.

5.2 Cross Correlation-Measure of Similarity

Assume two real time domain signals $x(n)$ and $y(n)$ are available. The samples are evaluated at discrete intervals and satisfy all discrete time sampling constraints. The cross correlation between these two signals is defined by

$$r_{xy}(\tau) = \sum_{n=-\infty}^{+\infty} x(n)y(n-\tau) \qquad 5.1$$

where τ is time shift or time delay parameter and the subscript xy indicates the signals used in the cross-correlation. Recall that the inner product of two vectors in a finite dimensional domain is

$$\langle x(n), y(n) \rangle = \sum_{n=0}^{N-1} x(n)y(n) \qquad 5.2$$

where $0 \le n \le N-1$ is the domain of interest.

Let $y(n) = x(n-\tau)$ in Equation 5.2. When τ=0, signal $x(n)$ and $x(n-\tau)$ are identical. The inner product (Equation 5-2) is at a maximum. In general, the shift parameter between two signals always occurs at the peak of cross correlation [Silvia, 1986]. Compared to Equation 5-2, the cross correlation (Equation 5-1) is actually the inner product of $x(n)$ and $y(n)$, which is a function of shift parameter τ. Therefore, the cross correlation, like other inner products, measures the degree of similarity between two signals. In general, the cross correlation function is neither symmetrical, nor unimodal [Silvia, 1986].

Figure 5.1 shows two signals and the corresponding cross correlation. In this case, $y(n)$ is indeed a delayed version of $x(n)$ ($y(n) = x(n-4)$). The peak of the cross correlation and its corresponding shift index ($\tau = -4$) show that the time shift between these two signals is –4, where the negative sign indicates $y(n)$ is being delayed by the $x(n)$.

5.3 Relative Time Delay Estimation

In this thesis, the method of cross correlation was used to measure the relative time delay to a reference signal that results from the wave propagation through a water path. An unknown signal, which is from the wave that has propagated through the sample, is used in the computation. The relative time delay is determined by locating the time at which the cross-correlation r_{xy} is at a maximum. This is the point

when the signals are most similar. The (average group) phase velocity V of the ultrasonic waves propagating through the sample, introduced in Section 3.5.2, can be estimated by

$$V_i(x_1,\varphi) = \frac{V_0}{\sqrt{1+\frac{V_0\tau_i}{d}\left[\frac{V_0\tau_i}{d}-2\cos\theta_i\right]}} \qquad 5.3$$

where V_0 is the wave velocity in the water, τ_i is time delay, θ_i is the incident angle, d is the thickness of the sample, and (x_1, φ) indicts the wave incident plane (Section3.5.2).

Because the specimen used is quite thin, material dispersion from the visco-elasticity of the material is not significant [Peterson, 1997]. In addition, the specimen is of sufficient width that there is no significant geometric dispersion present in the

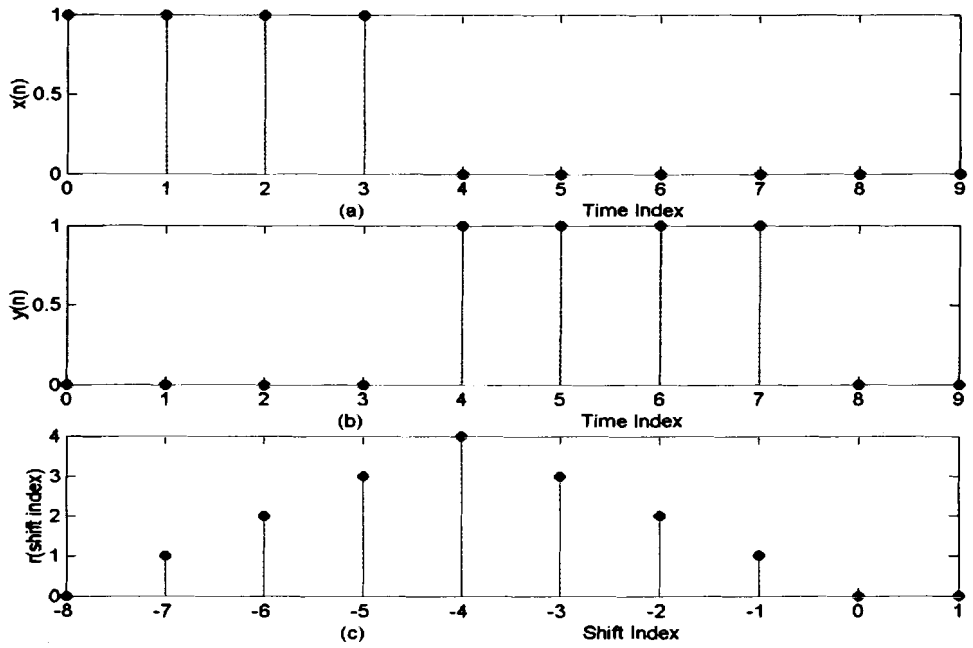

Figure 5.1. Cross correlation. (a) signal x(n); (b) signal y(n) =x(n-4); (c) cross correlation r_{xy} between x(n) and y(n).

signals. It is important to note that the use of the cross correlation results only in a measure of the relative difference in the velocity. Therefore, the cross correlation can be used to determine the difference in wave velocity between the reference sample and the unknown sample. For the range of velocities considered, the only geometrical dispersion that would only impact the measurement exists if large differences in the phase velocities present between the unknown and the reference signal [Peterson, 1997]. As a result, unlike absolute measurements of velocity even in finite specimens, the effect of dispersion can be assumed to be minimal. Figure 5.2 gives an illustration of the cross-correction between the reference signal (ultrasonic pulser in water) and the unknown sample (ultrasonic pulser through aluminum oxide immersed in water).

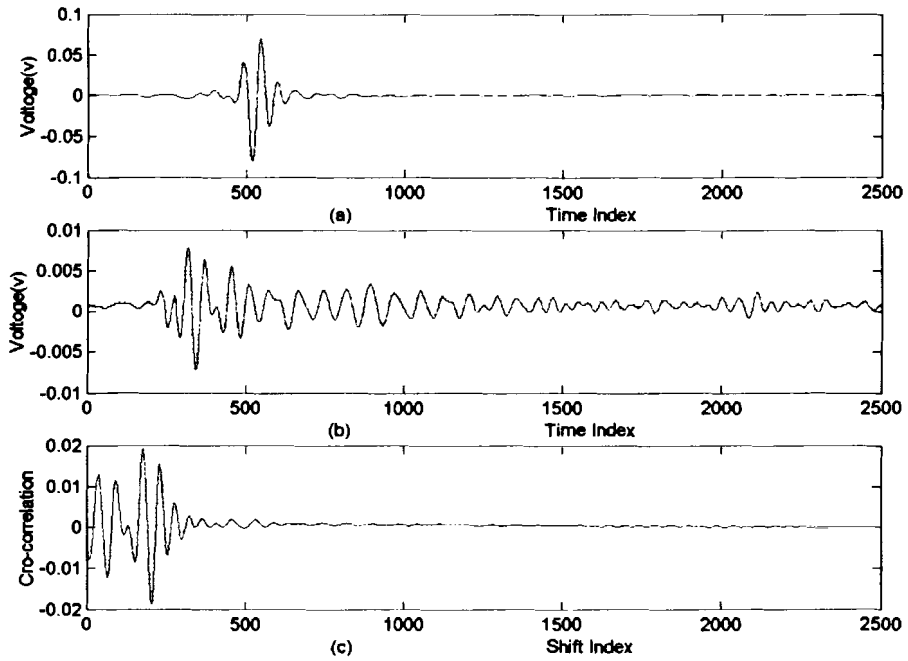

Figure 5.2. A plot of cross correlation. (a) a reference signal (signal through water only); (b) an unknown signal (signal through aluminum oxide); (c) cross correlation between (a) and (b).

6 EXPERIMENTAL SYSTEM

6.1 Experimental Setup

The experimental arrangement used is shown in Figure 6.1. Two matched immersion transducers with center frequency of 2.25 MHz (Parametric, Model v306) are placed on each side of the sample. One is the transmitting transducer (a focused transducer with a diameter of 12mm) and the other is a receiving transducer (a flat transducer with a diameter of 12mm). The position of the transmitting transducer is fixed along the center of the sample. The position of the receiving transducer is adjusted manually to the peak of the signal. Alternatively, it is possible to compute the position using Snell's law [Hosten, 2001]. To ensure that the measurements are performed in different directions, a plate of the sample (aluminum oxide, Alfa Aesar), with a diameter of 25.4 mm and a thickness of 3.4 mm, is obtained and mounted onto

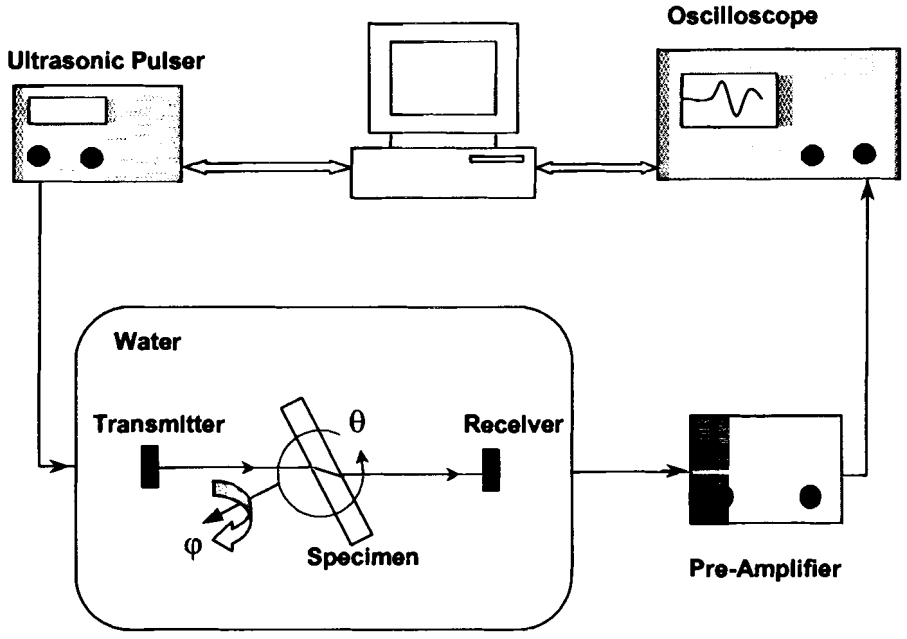

Figure 6.1. A schematic drawing of the experimental system for measuring elastic constants with immersion method.

a goniometer to adjust the angles. The azimuthal angle φ, which characterizes the incident plane is varied manually and the incident angle θ is controlled by the goniometer, respectively.

A photograph of the experimental set up is given in Figure 6.2.

6.2 Experimental Measurements

An ultrasonic signal is generated by an electronic pluser/receiver (Parametrics, Model 5072 PR), which excites a piezoelectric transducer with a center frequency of 2.25 MHz and a diameter of 12 mm. The wave is obliquely incident onto the sample surface and is transmitted through the sample with mode conversion depending on the angles. The signal is received by a piezoelectric transducer and then amplified by a pre-amplifier (Parametrics, Model 5662). The received signal is averaged and

Figure 6.2. A photograph of the experiment setup for measuring the elastic constants with the through-transmission technique. The left top shows the testing sample, a single crystal of aluminum oxide, in this system.

digitized by a digital oscilloscope (Tektronix, Model TDS 520A). Signals are transferred to a personal computer. All the measurements were conducted in a water tank where the temperatures were monitored by an ATD prose.

The measurements were performed with 4 incident planes (x_1, φ), where azimuthal angle $\varphi=0^0$, 45^0, 90^0, 135^0 associated at a range of different incident angles. In each of the incident planes, 25 measurements were carried out corresponding to 25 incident angles (0^0 to 24^0). At each incident angle, the relative time delay was measured from the signals received. Only the highest amplitude mode, which contained higher energy indeed, was measured. The two quasi-transverse modes in some cases have such similar arriving time that, at certain angles, the signals overlap. Overlapping signals has the potential to complicate the characterization and make the distinction of the two modes very difficult. However, the immersion ultrasonic technique and the optimization algorithm do not require that the QL, QT1 or QT2 be distinguished. Therefore, the determination of the elastic constants from the measured velocity data is more straightforward than the signals suggest.

To determine phase velocity of the received signal through the sample, cross correlation was performed between the reference and unknown signal. The reference signal was obtained by aligning the two transducers and placing them parallel at a distance, which allows the sample to be placed between the transducers. The reference signal is acquired by measuring the water path without placing the sample between them. The velocity can be found from

$$V_i(x_1,\varphi) = \frac{V_0}{\sqrt{1+\frac{V_0\tau_i}{d}\left[\frac{V_0\tau_i}{d}-2\cos\theta_i\right]}} \qquad 6.1$$

where V_0 was the reference velocity at the measured temperature.

6.3 Choice of Sample Material

The immersion ultrasonic through-transmission technique, as well as the optimization routine presented, are applicable regardless of the symmetry groups of the materials. Theoretically, any homogeneous anisotropic material can be used in this work. However, there are some further restrictions involved, such as solubility of the material in water, physical size and available geometry of the material. With these constraints, a single crystal of aluminum oxide (Medal base, 99.9%, Alfa Aesar) was selected. Aluminum oxide has a trigonal system with 6 independent elastic constants. Handbook values for the properties of the sample are used [Hellwege, 1979] as the initial guess for the optimization algorithm as well as for result comparison. The elastic constants in GPa are

$$C = \begin{bmatrix} 495 & 160 & 115 & -23 & 0 & 0 \\ & 495 & 115 & 23 & 0 & 0 \\ & & 497 & 0 & 0 & 0 \\ & & & 146 & 0 & 0 \\ & sym. & & & 146 & -23 \\ & & & & & 167.5 \end{bmatrix} GPa \qquad 6.2$$

where

$$\begin{aligned} C_{44} &= C_{55} \\ C_{14} &= -C_{24} = C_{56} \\ C_{66} &= \frac{1}{2}(C_{11} - C_{12}) \end{aligned} \qquad 6.3$$

The specimen geometry is a parallel disk with diameter of 25.4 mm and a thickness of 3.2 mm. The specimen has random axis orientation so that the

optimization algorithm can be tested as well as the technique to find the misorientation between the measurement axes and the material axes. Since handbook properties are available, reasonable accuracy can be determined.

7 RESULTS AND DISCUSSIONS

The ultrasonic phase velocities for 25 signals in the four incident planes ($\mathbf{x}_1$, φ), $\varphi=0^0$, 45^0, 90^0, 135^0, were calculated from the measured time delay using Equation 6.1. An observation coordinate system $R = (x_1, x_2, x_3)$ was set up such that $\mathbf{x}_1$ was normal to the sample plate; $\mathbf{x}_2$ and $\mathbf{x}_3$ were as shown in Figure 7.1. The origin of the coordinate system R was set at the center of the sample.

7.1 Results of Measured Phase Velocities

Results of the measured phase velocities are shown as a function of incident angle θ_i, where i= $0^0 \ldots 24^0$ in Figure 7.2. The theoretical phase velocities calculated from the reconstructed elastic constants are compared with the experimental data in Figure 7.2. The measured data are seen as starting points and the solid lines are calculated values. Figure 7.2 shows that the experimental data matches well with the calculated phase velocity curves.

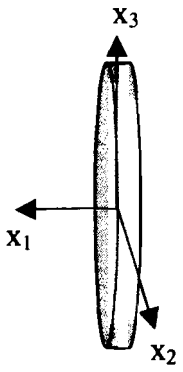

Figure 7.1. An observation coordinate system R=(x_1, x_2, x_3) for ultrasonic measurements.

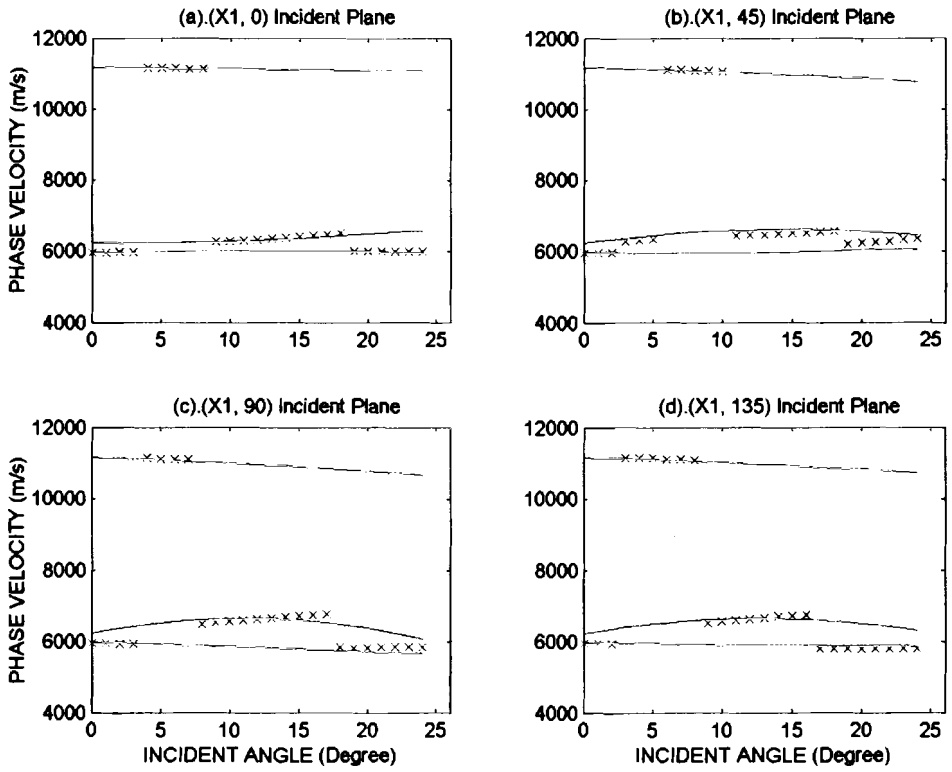

Figure 7.2. Phase velocity (in m/s) for an Al_2O_3 single crystal verse incident angle measured in (a) (x_1, 0^0), (b) (x_1, 45^0), (c) (x_1, 90^0), (d) (x_1, 135^0) incident planes. The starting points are experimental data. The three solid lines are phase velocities corresponding to wave modes QL, QT1 and QT2, respectively, which are calculated from the reconstructed elasticity constants.

7.2 Results of Reconstructed Elastic Constants

Results of the elastic constants (in GPa) that are reconstructed from the velocity data measured in the observation coordinate system R are

$$[C]=\begin{bmatrix} 471.184 & 158.660 & 135.140 & -45.982 & 0.1091 & 0.0010 \\ & 492.222 & 118.221 & 3.444 & 00.4033 & 0.3800 \\ & & 348.080 & 4.033 & 0.6200 & 0.1006 \\ & & & 140.930 & 0.4420 & 0.4801 \\ & sym. & & & 41.410 & -81.340 \\ & & & & & 143.020 \end{bmatrix} GPa \quad 7.1$$

Two eigenvectors of tensor A (Voigt tensor, section 4.1) and B (dilatational modulus), respectively, are

$$[Vec\_A]=\begin{bmatrix} -0.0074 & -0.9996 & -0.0275 \\ 0.2137 & 0.0254 & -0.9766 \\ 0.9769 & -0.0128 & 0.2162 \end{bmatrix}$$

$$[Vec\_B]=\begin{bmatrix} -0.0096 & -0.9999 & -0.0040 \\ 0.2674 & 0.0013 & -0.9636 \\ 0.9635 & -0.0101 & 0.2673 \end{bmatrix} \quad 7.2$$

As noted previously, due to the experimental errors the eigenvectors of A and B are not exactly identical. To determine the symmetry planes the material possess, the angular deviations between each pair of eigenvectors are calculated. The eigenvector pair that exhibits the small angular deviation is considered to be a good estimate of a normal to a symmetry plane (see section 4.1).

Three angular deviations between each pairs of eigenvectors are

$$\theta_1 = 3.03^0, \theta_2 = 1.40^0, \theta_3 = 3.35^0 \quad 7.3$$

Equation 7.3 shows that each angular deviation may be considered to be small enough to conclude that three symmetry planes exist within the tested material. Recall

that the original values from the material handbook shows that three perpendicular symmetry planes exist in a trigonal material. This can be independently verified by using X-ray scatting technique. Thus, the material symmetry can be assumed to be known. The average of the two vectors V_i^{ave} (i=1, 2, 3) (Equation 7.2) associated with the eigenvector pairs is used as good estimates of the normals to the symmetry planes.

$$V^{ave} = \begin{bmatrix} -0.0087 & -1.0000 & -0.0158 \\ 0.2405 & 0.0134 & -0.9701 \\ 0.9702 & -0.0115 & 0.2418 \end{bmatrix} \tag{7.4}$$

Thus, the three unit vectors of the normals to the symmetry planes with respect to the observation coordinate system R are

$$\begin{aligned} e_1 &= -0.0087x_1 + 0.2405x_2 + 0.9702x_3 \\ e_2 &= -1.0000x_1 + 0.0134x_2 - 0.0115x_3 \\ e_3 &= -0.0158x_1 - 0.9701x_2 + 0.2404x_3 \end{aligned} \tag{7.5}$$

where $\mathbf{x_1}$, $\mathbf{x_2}$, $\mathbf{x_3}$ are unit base vectors of the observation coordinate system R.

7.3 Results of Estimation of Principal Coordinate System

As introduced in section 4.2, the principal coordinate system R^P with respect to the observation coordinate system R can be located by determining a set of Euler's angle unknowns $\delta=(\alpha, \beta, \gamma)$ with at least one of the unknown is zero [Auld, 1990, and Aristegui, 1997]. V_3^{ave} was used to extract the Euler's angles.

$$\begin{aligned} e_3 &= -0.0158x_1 - 0.9701x_2 + 0.2404x_3 \\ &= \cos(\alpha)x_1 - \sin(\alpha)\cos(\beta)x_2 + \sin(\alpha)\sin(\beta)x_2 \end{aligned} \tag{7.6}$$

Thus, a set of Euler's angles are

$$\alpha \cong 90.9^0$$
$$\beta \cong 14.0^0 \qquad 7.7$$
$$\gamma = 0$$

Therefore, the principal system R^P was determined by a rotation through a counterclockwise angle $\alpha=90.9^0$ about the x_3 axis followed by another counterclockwise rotation through an angle $\beta=14.0^0$ about the *transformed* $\mathbf{x_1}$. Figure 7.3 (b) shows the location of the principal system R^P with respect to its observation coordinate system R. The rotation is associated with the corresponding Euler angles α and β. Figure 7.3 (a) gives an illustration of the orientation of the V_3^{ave}, which is one of the normals to the symmetry planes. It should be noted that the Euler's angles could also be determined by V_1^{ave}.

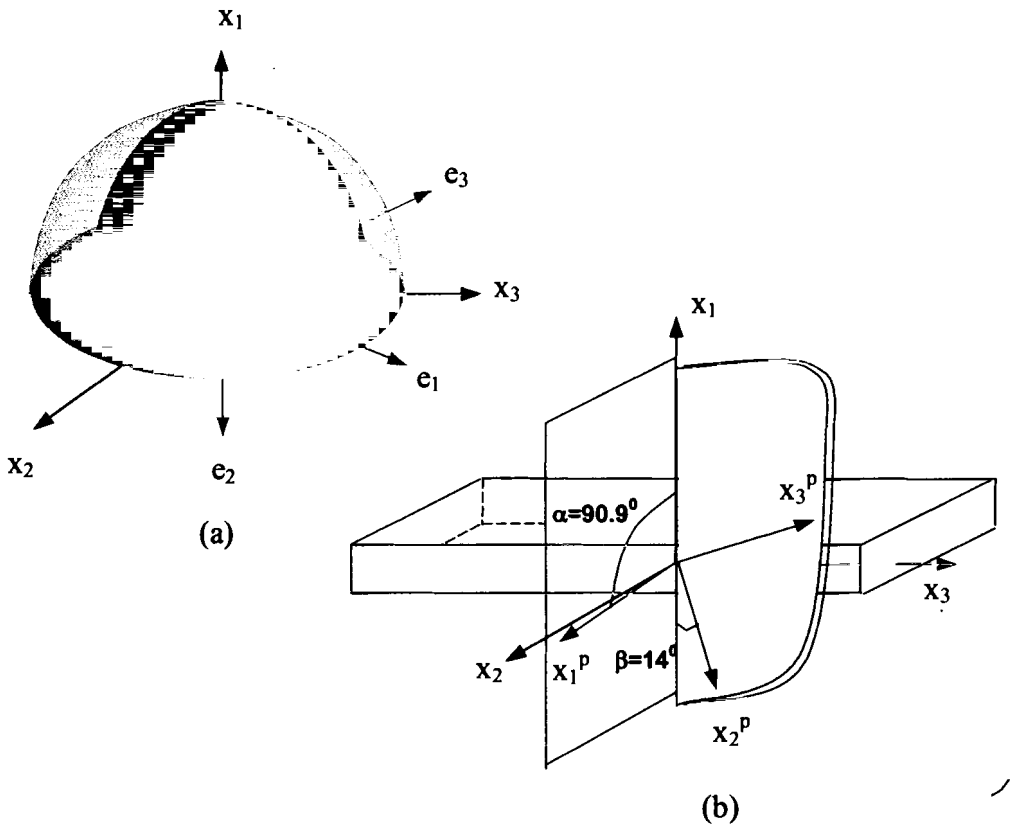

Figure 7.3 (a). An illustration of normals to the symmetry planes for a single crystal of aluminum oxide in an observation coordinate system R. (b). Location of the principal coordinate system R^p (x_1^p, x_2^p, x_3^p) with respect to its observation coordinate system R associated with the Euler angles $\alpha=90.9^0$ and $\beta=14^0$.

The elastic constants C^P referred to its principal coordinate system R^P can be determined by applying tensor transformation law (Equation 3.12), which is

$$C'_{mnop} = a_{mi} a_{nj} a_{ok} a_{pl} C_{ijkl} \qquad 7.8\ (3.12)$$

where [a] is a [3×3] transformation matrix whose numerical components were found based on the estimated Euler angles.

Two transformations have been carried out corresponding to two Euler's angles to determine the C^P, respectively. From (3.12), (3,13) and (3.14), C^P (in GPa) in coordinated system R^P is:

$$[C^p] =$$

$$\begin{bmatrix} 478.5(495) & 178.9(160) & 121.9(115) & -1.882(-23) & -23.54(0) & 0.801(0) \\ & 471.9(495) & 114.9(115) & 2.063(23) & 35.02(0) & 0.910(0) \\ & & 354.5(497) & 0.210(0) & -13.33(0) & 0.110(0) \\ & & & 9.170(146) & 2.139(0) & 47.87(0) \\ & \textit{sym.} & & & 144.5(146) & -1.681(-23) \\ & & & & & 175.3(168) \end{bmatrix}$$

7.9

The numbers in the parenthesis in Equation 7.9 are the elastic constants obtained from a material handbook [Hellwege, 1979]. Comparison of these values finds that reconstructed values of C_{11}, C_{12}, C_{13}, C_{16}, C_{22}, C_{23}, C_{26}, C_{34}, C_{36}, C_{45}, C_{55}, C_{66} match well with the handbook values.

The reason for the large difference for the remaining may be explained by the following. For a trigonal material, in addition to the three perpendicular symmetry planes, a symmetry axis also exists. Any of the $\vec{x_1}, \vec{x_2}, \vec{x_3}$ coordinate axes can be symmetry axis. The handbook value shows that the $\vec{x_1}$ is the symmetry axis. This is because C_{14}, C_{24}, C_{56} are non-zeros. However the result in Equation 7.9 indicates that

$\overrightarrow{x_2}$ may potentially be the symmetry axis in this coordinate system setup. The conclusion may be verified from that one of the Euler's angles α is roughly 90^0.

The result shown in Equation 7.9 can be verified by finding the normals to the symmetry planes with respect to the constructed principal coordinate system R^P. In other words the closest of eigenvectors of the tensor A and B determined by the components of C^P with respect to its coordinate system R^P should be the unit base vectors of coordinate system R^P tself (see section 4.1). This feature can be easily drawn from the following calculations. The unit vectors of the normals to the symmetry planes in coordinate system R^P determined by C^P are

$$\begin{aligned} e_1 &= -0.014x_1{}^P - 0.000x_2{}^P + 0.999x_3{}^P \\ e_2 &= -0.016x_1{}^P + 0.999x_2{}^P - 0.000x_3{}^P \\ e_3 &= -0.999x_1{}^P - 0.016x_2{}^P - 0.014x_3{}^P \end{aligned} \qquad 7.10$$

If the experimental errors are taken into count, the $e_i\,(i=1,2,3)$ in Equation 7.10 actually line up with the three unit vectors $x_i{}^P\,(i=3,2,1)$ of R^P, respectively, which indeed characterizes the feature of that the normals to the symmetry planes in its principal coordinate system are the unit base vectors of the coordinate system itself.

7.4 Results with Carbon-Carbon Composites

Testing was also carried out with the carbon-carbon composite materials. The carbon-carbon samples used were supplied by Applied Thermal Science, Inc. Four samples were tested, each of which was a rectangular parallelepiped in 25.4×25.4 mm with a thickness of 6mm. The testing procedures were exactly the same with the

aluminum oxide described previously. The initial guesses for the carbon-carbon were measured by applying a contact technique for ultrasonic measurement from the primary work [Sun and Peterson, 2001], where the material was assumed to be an orthotropic material. A Cartesian coordinate system R is set up in such a way that the coordinate axes are parallel to the geometric axes of the sample.

A set of initial guess (in GPa) used for carbon-carbon was obtained from the initial work [Sun, M. and Peterson, M. 2001], where a contact technique [Buskirk et al, 1986] was applied for ultrasonic measurement.

$$[C]=\begin{bmatrix} 47.60 & 8.000 & 6.000 & 0 & 0 & 0 \\ & 18.91 & 4.000 & 0 & 0 & 0 \\ & & 18.84 & 0 & 0 & 0 \\ & & & 3.111 & 0 & 0 \\ & sym. & & & 5.213 & 0 \\ & & & & & 4.534 \end{bmatrix}$$

One of the results of the elastic constants (in GPa) for the carbon-carbon sample reconstructed from the velocity data in the observation coordinate system R are

$$[C]=\begin{bmatrix} 47.44 & 8.003 & 6.001 & 0.052 & -0.207 & 0.000 \\ & 18.72 & 4.210 & 0.001 & 0.136 & 0.001 \\ & & 18.47 & 0.347 & 0.139 & 0.026 \\ & & & 4.730 & 0.505 & 0.396 \\ & sym. & & & 5.162 & 0.638 \\ & & & & & 4.371 \end{bmatrix} \qquad 7.11$$

As with the aluminum oxide, identification of the symmetry planes as well as determination of its principal coordinate frame R^P were also carried out. Three symmetry planes exist in the material. A set if Euler's angles corresponding to R with respect to R^P in this sample is

$$\alpha \cong 179.2^0$$
$$\beta \cong 78.7^0 \qquad 7.12$$
$$\gamma = 0$$

The misorientation between the geometric axes $\mathbf{x}_1$, $\mathbf{x}_2$, $\mathbf{x}_3$ and the symmetric axes $\mathbf{x}_1^P$, $\mathbf{x}_2^P$, $\mathbf{x}_3^P$ are shown in Figure 7.4.

The elastic constants C^P referred to its principal coordinate system R^P in GPa are

$$[C^P] = \begin{bmatrix} 47.75 & 6.718 & 7.281 & -0.963 & 0.121 & -0.273 \\ & 15.821 & 6.621 & 0.383 & 0.507 & 0.023 \\ & & 16.56 & -0.421 & -0.705 & -0.259 \\ & & & 7.138 & -0.113 & -0.013 \\ & \text{sym.} & & & 4.049 & 0.239 \\ & & & & & 5.482 \end{bmatrix}$$

Results of the reconstructed elastic constants in the principal coordinate system for the carbon-carbon samples are listed in Table 7.1, including the one shown

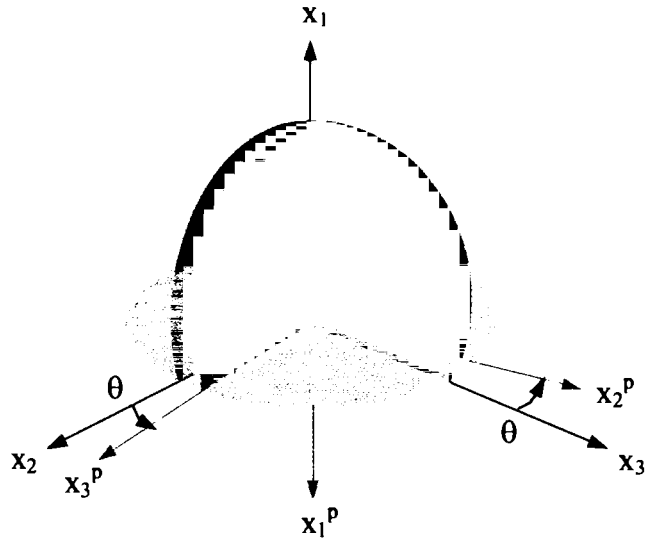

Figure 7.4. An illustration of the misorientation between the geometric axes x_1, x_2, x_3 and the symmetric axes x_1^P, x_2^P, x_3^P with $\theta=11.3^0$ for a carbon-carbon composite.

above. Table 7.1 shows that the misorientation between the geometric axes and the symmetric axes vary from sample to sample.

Table 7.1. Results of elastic constants and the associated Euler's angles with the carbon-carbon composite material.

C_{ij}		initial data	sample 1	sample 2	sample 3
C_{11}		47.60	47.75	48.16	47.60
C_{12}		8.000	6.718	7.594	7.556
C_{13}		6.000	7.281	6.838	7.844
C_{14}		0	-0.963	0.001	-0.263
C_{15}		0	0.121	0.000	-0.000
C_{16}		0	-0.273	0.001	-0.001
C_{22}		18.91	15.82	19.04	15.14
C_{23}		4.000	6.621	4.390	6.713
C_{24}		0	0.383	0.000	2.017
C_{25}		0	0.507	-0.959	0.000
C_{26}		0	0.023	0.001	0.001
C_{33}		18.84	16.56	24.90	15.18
C_{34}		0	-0.421	-0.151	-2.047
C_{35}		0	-0.705	1.596	0.000
C_{36}		0	-0.260	-0.001	0.000
C_{44}		3.111	7.138	8.223	6.824
C_{45}		0	-0.113	-5.320	0.000
C_{46}		0	-0.013	-1.431	-0.001
C_{55}		3.218	4.049	13.86	4.717
C_{56}		0	0.239	0.001	-0.299
C_{66}		4.537	5.482	4.525	5.041
Euler's angles	α	N/A	179.2^0	85.7^0	1.5^0
	β	N/A	78.7	175.5^0	1.7^0
numbers of symmetry planes		3 perpendicular symmetry planes	3 perpendicular symmetry planes	1 symmetry plane	3 perpendicular symmetry planes
deviation of geometric axes from symmetric axes		0^0	11.3^0	4.5^0	1.7^0

8 CONCLUSIONS AND FUTURE WORK

From the work described in this thesis, several conclusions can be drawn.

- A water immersion method to optimally recover the elastic constants for a general anisotropic material has been demonstrated. The approach is based on wave velocity measurements and a Newton-Raphason nonlinear optimization.
- Identification of material symmetries and the corresponding principal coordinate system has been introduced.
- The recovery of the Euler's angles is tested for the case of two angular unknowns.
- Numerical as well as experimental results show the method introduced in this work is effective and applicable.

Future work can focus on the stability of the optimization algorithm. This is a quite straightforward procedure since it only involves applying some random scatter on the initial guess and on the measured velocity data. Another extension to this work is to investigate the sensitivity of this elastic constant determination for weak and strong anisotropies. This can be done by using both numerical and experimental data from various materials that possess different symmetry classes.

Finally two other directions are useful. Many materials have not been challenged completely by a method such as the one shown. For specimens ranging from wood to composites, many interesting results are expected. Further work will also consider extending the determination of symmetry class to non-Cartesian

samples. This is an interesting problem and is with relevance to a range of natural and man-made materials.

REFERENCES

Aristegui, C. and Baste, S., "Determination of the elastic symmetry of a monolityic ceramic using bulk acoustic waves." J. Nondestructive Evaluation. Vol. 19, pp. 115-126. 2000.

Aristegui, C. and Baste, S., "Optimal determination of the material symmetry axes and associated elasticity tensor from ultrasonic velocity data." J. Acoust. Soc. Am. Vol. 102 (23), pp. 1503-1521. 1997.

Auld, B. A., *Acoustic Fields and Waves in Solids.* Vol.1, Chapter 3, pp.57-82. Krieger Publishing Comp. Malabar, FL. 1990.

Bond, W., "The Mathematics of the Physical Properties of Crystals." BSTJ. Vol. 22, pp. 1-72. 1943.

Borgnis, F. E., "Specific directions of longitudinal waves propagation in anisotropic media." Phys. Rev. Vol. 98, pp. 1000-1005. 1955.

Chimenti, D.E., "Guided waves in plates and their use in materials characterization." J. Am. Soc. Mech. Eng, Vol. 50 (5), pp.247-284. 1997.

Chu, Y. C., Degtyar, A.H., and Rokhlin, S. I., "A method for determination of elastic constants of a unidirectional lamina from ultrasonic bulk velocity measurements." J. Acoust. Soc. Am. Vol. 96, pp. 342-352. 1994.

Chu, Y. C., Degtyar, A.H., and Rokhlin, S. I., "Stability of determination of composite moduli from velocity data in planes of symmetry for weak and strong anisotropies." J. Acoust. Soc. Am. Vol. 95, pp. 213-225. 1994.

Cowin, S. C. and Mehrabadi, M. M., "On the identification of material symmetry for anisotropic elastic materials." Q. J. Mech. Appl. Math. Vol. 40, pp. 451-476. 1987.

Cowin, S. C., "Identification of elastic material symmetry by acoustic measurement". *Elastic Wave Propagation.* Editors: McCarthy, M. F. and Hayes, M. A. Elsevier Science Publishers. B.V. North-Holland. 1989.

Cowin, S. C., "Properties of the anisotropic elasticity tensor." Q. J. Mech. Appl. Math. Vol. 42, pp. 249-266. 1989.

Every, A. G. and Saches, W., "Determination of the elastic constants of anisotropic solids from axoustic-wave group-velocity measurements." Physics Review. Vol. B42, pp. 8196-8205. 1990.

Every, A. G. and Saches, W., "Sensitivity of inversion algorithms for recovering elastic constants of anisotropic solids from longitudinal wavespeed data." Ultrasonic. Vol. 30, pp. 43-48. 1992.

Every, A. G., and Schase, W., *Handbook of Elastic Properties of Solids, Liquids, and Gases*. Vol. I, "Dynamic methods for measuring the elastic properties of solids", (chief) Editors: Levy, M., Bass, H., and Stern, R. R. Academic Press. New York. 2001.

Fedorov, F. I., *Theory of Elastic Waves in Crystals*. Chapter 3, pp. 85-97. Plenum Press. New York. 1986.

Flint, E.E., *Principles of Crystallography*. Chapter 3, pp. 56-67. Mir Publishers. Moscow. 1952.

Frederick, D., Chang, T. S., *Continuum Mechanics*. Chapter 3, pp. 45-49. Allyn and Bacon, Inc. Boston. 1965

Hearmon, R. F. S., *An Introduction to Applied Anisotropic Elasticity*. Chapter 6, pp. 68-79. Oxford University Press. London. 1961.

Hellwege, K. H., (chief) Editor. *Numerical Data and Functional Relationships in Science and Technology*. Chapter 3, pp. 44-47. New Series. Springer-Verlag Berlin. 1979.

Hellwege, K. H., (chief) Editor. *Numerical Data and Functional Relationships in Science and Technology*. Vol. 11. Springer-Verlag Berlin. Heidelberg. New York. 1979.

Hosten, B., "Reflection and transmission of acoustic plane waves on an immersed orthotropic and viscoelastic solid layer." J. Acoust. Soc. Am. Vol. 89, pp. 2745-2752. 1991.

Hosten, B., "Ultrasonic Through-Transmission Method for measuring the complex stiffness moduli of composite materials." *Handbook of Elastic Properties Solids, Liquids, and Gases*. Chapter 3, pp. 67-70. Academic Press. New York. 2001.

Khathevich, A. G., "The acoustic axis in crystals." Sov. Phys. Crystallogr. Vol. 7, pp. 601. 1962.

Kunz, K. S., *Numerical Analysis*. Chapter 1, pp. 10-14. McGraw-Hill Company, Inc. New York. 1957.

Lee, W. Y., and Koc, W.C., "On the determination of the elastic of tetragonal crystal with application to strontium molybdate." Solid State Commun. Vol. 70, pp. 459. 1989.

Markham, M. F., "Measurement of the elastic constants of fiber composites by ultrasonics." Composites. Vol. 11, pp. 145-149. 1970.

McSkimin, H. J. J., "Pulse superposition method for measuring ultrasonic wave velocities in solid." Acoust. Soc. Am. Vol. 33, pp. 12. 1961.

McSkimin, H. J., J., "Measurement of ultrasonic velocities and elastic moduli for small solid specimens at high temperature." Acoust. Soc. Am. Vol. 31, pp. 287. 1959.

Meyer, S., *Data Analysis for Scientist and Engineer.* Chapter 33, pp. 387-400. John Wiley & Sons, Inc. New York, 1975.

Migliori, A., and Sarrao, J. L, *Resonant ultrasound spectroscopy,* Chapter 1, pp. 13-14. Wiley, New York, 1997.

Musgrave, M. J. P., *Crystal Acoustics.* Chapter 6, pp. 68-86. Holden-Day, Inc. San Francisco. 1970.

Nadeau, G., *Introduction to Elasticity.* Chapter 2, pp. 61-65. Holt, Rinehart and Winston. New York. 1964.

Neighbours, J. R., J. Appl. Phys. Vol. 51, pp. 5801-5803. 1980.

Norris, A. N., "On the acoustic conditions for the existence of symmetry planes." Q. J. Mech. Appl. Math. Vol. 42, pp. 412-426. 1989.

Papadakis, E. P., Patton, T., Tsai, Y. M., Thompson, D. O., and Thompson, R. B., "The elastic moduli of a thick composite as measured by ultrasonic bulk wave pulse velocity." J. Acoust. Soc. Am. Vol. 89, pp. 2753-2757. 1991.

Peterson, M. L., "A Method for Increased Accuracy of the Measurement of Phase Velocity." Ultrasonic. Vol. 35 (1), pp. 17-29. 1997.

Pierre, D. A., *Optimization Theory with Applications.* Chapter 1, pp. 20-24. John Wiley & Son, Inc. New York. 1969.

Proakis, J. G, and Manolakis, D. G., *Digital Signal Processing* (3rd edition). Prentice-Hall. New Jersey. 1996.

Rokhlin, S. I. and Wang, W., "Double through-transmission bulk surface wave method for ultrasonic phase velocity measurement and determination of elastic constants of composite materials." J. Acoust. Soc. Am. Vol. 91, pp. 3303-3312. 1992.

Schreiber, E., Aderson, O., and Soga, N., *Elastic Constants and their Measurements.* Chapter 2, pp. 19-26. McGraw-Hill. New York, 1973.

Shames, I. H., *Engineering Mechanics*. Vol. II. Dynamics. Chapter 19, pp. 653-655. Prentice-Hall, Inc. New Jersey, 1966.

Silvia, M. T., "Time Delay Estimation." *Handbook of Digital Signal Processing*. Chapter 11, pp. 822-830. Editor: Elliott, D. F. Academic Press, Inc. New York. 1986.

Sun, M. and Peterson, M., "Visco-Elastic constant recovery in the absence of known material symmetry." Review of QNDE, Vol. 21 B, pp. 1423-1430, Editors: Thompson, D. O. and Chimenti, D. E. American Institute of Physics. New York. 2001.

Van Buskirk, W. C. and Cowin, S. C., "A theory of acoustic measurement of the elastic constants of a gereral anisotropic solid." J. Materials Science. Vol. 21, pp. 2749-2762. 1986

Van Buskirk, W. C., Cowin, S. C. and Carter J. R., " A Theory of acoustic measurement of the elastic constants of general anisotropic solid." Journal *of* Materials Science, Vol. 21, pp. 2759-2762. 1986.

APPENDIX A. TENSOR CONVERSION FROM C_{IJKL} TO C_{IJ}

A. 1 Background

The constitutive equation, Hooke's Law, states that the stress σ_{ij}, a second order three dimensional tensor, is linearly proportional to the strain ε_{ij}, another second order three dimensional tensor, and vice versa. In general [Auld, 1997]

$$\begin{aligned} \sigma_{ij} &= C_{ijkl}\varepsilon_{kl} \\ \varepsilon_{ij} &= s_{ijkl}\sigma_{kl} \end{aligned} \qquad \text{A.1.}$$

where C_{ijkl} are elastic constants, s_{ijkl} are compliance constants. They are both fourth order three dimensional tensors.

Tensor transformation law is also applicable to σ_{ij}, ε_{ij} and C_{ijkl}, which are

$$\sigma_{mn}' = a_{mi}a_{nj}\,\sigma_{ij} \qquad \text{A.2.}$$

$$\varepsilon_{op}' = a_{ok}a_{pl}\,\varepsilon_{kl} \qquad \text{A.3.}$$

$$C'_{mnop} = a_{mi}a_{nj}a_{ok}a_{pl}\,C_{ijkl} \qquad \text{A.4.}$$

where a_{ij} is a [3×3] transformation matrix, whose physical quantities are direction cosines of the transformed coordinate axes with respect to its initial coordinate axes.

It is obvious from Equation A.4 that complicated algebraic manipulation exists when using Equation A.4 to obtain elastic constants in a transformed coordinate system. Therefore, it is of considerable importantance to perform coordinate transformations directly in an abbreviated subscript notation (second order six-dimensional tensor C_{ij}) without the effort required to convert to full subscripts (fourth order three-dimensional tensor C_{ijkl}), and reconvert back to the abbreviated notation after applying the transformation law. An efficient method for this purpose is

described in this section. The method was initially developed by Bond, W. L. [Bond, 1943]. It involves using the abbreviated notions for the stress tensor σ_{ij} and the strain tensor ε_{ij}. It also involves construction of a [6×6] transformation matrix $[M]$, which is obtained by performing the tensor transformation law. To avoid confusion, upper case letters are used to denote abbreviated subscripts (σ_I, ε_J, C_{IJ}) and lower case letters are for full subscripts (σ_{ij}, ε_{ij}, C_{ijkl}). But it should be noted that all the subscripts are indeed dummy variables, there are in fact no differences between them.

A. 2 Abbreviated Notations for σ_{ij}, ε_{ij}, and C_{ijkl}

Since both σ_{ij} and ε_{ij} are symmetric, each component can be specified by one subscript rather than two. Abbreviated notions are defined by

$$[\sigma]=\begin{bmatrix}\sigma_{11} & \sigma_{12} & \sigma_{13}\\ \sigma_{12} & \sigma_{22} & \sigma_{23}\\ \sigma_{13} & \sigma_{23} & \sigma_{33}\end{bmatrix}=\begin{bmatrix}\sigma_1 & \sigma_6 & \sigma_5\\ \sigma_6 & \sigma_2 & \sigma_4\\ \sigma_5 & \sigma_4 & \sigma_3\end{bmatrix} \qquad \text{A.5.}$$

$$[\varepsilon]=\begin{bmatrix}\varepsilon_{11} & \varepsilon_{12} & \varepsilon_{13}\\ \varepsilon_{12} & \varepsilon_{22} & \varepsilon_{23}\\ \varepsilon_{13} & \varepsilon_{23} & \varepsilon_{33}\end{bmatrix}=\begin{bmatrix}\varepsilon_1 & \frac{1}{2}\varepsilon_6 & \frac{1}{2}\varepsilon_5\\ \frac{1}{2}\varepsilon_6 & \varepsilon_2 & \frac{1}{2}\varepsilon_4\\ \frac{1}{2}\varepsilon_5 & \frac{1}{2}\varepsilon_4 & \varepsilon_3\end{bmatrix} \qquad \text{A.6.}$$

where the order of numbering in the abbreviated system follows the cyclic pattern [Auld, 1970]. The convention of having factors $\frac{1}{2}$ is standard practice in theory of elasticity, which can simplify some key equations in the theory.

In this abbreviated subscript notations, σ_{ij} and ε_{ij} can be written as [6×1] matrixes.

$$[\sigma]=\begin{bmatrix}\sigma_1\\ \sigma_2\\ \sigma_3\\ \sigma_4\\ \sigma_5\\ \sigma_6\end{bmatrix};\quad [\varepsilon]=\begin{bmatrix}\varepsilon_1\\ \varepsilon_2\\ \varepsilon_3\\ \varepsilon_4\\ \varepsilon_5\\ \varepsilon_6\end{bmatrix} \qquad \text{A.7.}$$

Simply because of the symmetric properties of σ_{ij} and ε_{ij}, the following conditions hold

$$\begin{aligned} C_{ijkl} &= C_{ijlk} \\ C_{ijkl} &= C_{jilk} \end{aligned} \qquad \text{A.8.}$$

Therefore, the four subsrcipts of C_{ijkl} may be reduced to two C_{IJ} by using abbreviated subscript notation, where

I	$i\,j$
1	11
2	22
3	33
4	23 *or* 32
5	13 *or* 31
6	12 *or* 21

A.9.

Relationships between C_{ijkl} and C_{IJ} are obtained by considering individual terms in the constitutive equation (Equation A.1) [Auld, 1970]. For example,

$$\sigma_{12} = C_{1222}\,\varepsilon_{22}$$

Conversion of the stress and strain to abbreciated subscripts gives

$$\sigma_6 = C_{1222}\,\varepsilon_2 = C_{62}\,\varepsilon_2 .$$

Consequently,

$$C_{62} = C_{1222} .$$

Therefore, in general

$$C_{IJ} = C_{ijkl}. \qquad \text{A.10.}$$

In a similar way, the compliance constants s_{ijkl} are found to be

$$s_{IJ} = s_{ijkl} \times \begin{cases} 1 & for\ I\ and\ J = 1, 2, 3 \\ 2 & for\ I\ or\ J = 4, 5, 6 \\ 4 & for\ I\ and\ J = 4, 5, 6 \end{cases} \qquad \text{A.11.}$$

The differences between Equation A.9 and Equation A. 10 result from the factors of two shown in Equation A.5.

With the introduction of abbreviated subscripts, Hooke's law (Equation A.1) may be written as a matrix equation. A complete expression for Hooke's Law is

$$\begin{aligned} &\sigma_I = C_{IJ}\varepsilon_J \\ &\varepsilon_I = s_{IJ}\sigma_J \\ &I, J = 1, 2, 3, 4, 5, 6 \end{aligned} \qquad \text{A.12.}$$

Many advantages exist with the introduction of the abbreviated notions. One of these can be seen immediately from Equation A.11 that the compliance matrix [s] is simply the inverse of the stiffness matrix [c]. That is

$$[s]^{-1} = [C]$$

Another important result is that C_{IJ} and S_{IJ} in Equation A.11 are in fact higher dimensional tensors rather than matrices used for notation only. The feature of being higher dimensional tensors can be further drawn from the following section.

A. 3 Transformations with Abbreviated subscripts

Consider the stress σ_{ij}. In full subscript notation, the transformation law applies, which is

$$\sigma_{mn}' = a_{mi} a_{nj} \sigma_{ij} \qquad \text{A.13.}$$

where [a] is the [3×3] transformation matrix introduced previously.

To convert to abbreviated subscripts, each stress component must be examined individually. For example,

$$\begin{aligned}\sigma_{11}' = {} & a_{11}^2 \sigma_{11} + a_{11} a_{12} \sigma_{12} + a_{11} a_{13} \sigma_{13} \\ & + a_{21} a_{11} \sigma_{21} + a_{12}^2 \sigma_{22} + a_{12} a_{13} \sigma_{23} \\ & + a_{13} a_{11} \sigma_{31} + a_{13} a_{12} \sigma_{32} + a_{13}^2 \sigma_{33}\end{aligned}$$

Conversion of σ_{ij} to abbreviated notation σ_I gives

$$\sigma_1' = a_{11}^2 \sigma_1 + a_{12}^2 \sigma_{22} + a_{13}^2 \sigma_{33} + 2a_{12} a_{13} \sigma_4 + 2a_{11} a_{13} \sigma_5 + 2a_{11} a_{12} \sigma_6$$

Repetition of the same procedure for each component of σ_I' obtains the transformation law

$$\begin{aligned}&\sigma_I' = M_{IJ} \sigma_J \\ &I, J = 1, 2, 3, 4, 5, 6\end{aligned} \qquad \text{A.14.}$$

where M_{IJ} defines a [6×6] transformation matrix.

$$[M] = \begin{bmatrix} a_{11}^2 & a_{12}^2 & a_{13}^2 & 2a_{12}a_{13} & 2a_{13}a_{11} & 2a_{11}a_{12} \\ a_{21}^2 & a_{22}^2 & a_{23}^2 & 2a_{22}a_{23} & 2a_{23}a_{21} & 2a_{21}a_{22} \\ a_{31}^2 & a_{32}^2 & a_{33}^2 & 2a_{32}a_{33} & 2a_{33}a_{31} & 2a_{31}a_{32} \\ a_{21}a_{31} & a_{22}a_{32} & a_{23}a_{33} & a_{22}a_{33} + a_{23}a_{32} & a_{21}a_{33} + a_{23}a_{31} & a_{22}a_{31} + a_{21}a_{32} \\ a_{31}a_{11} & a_{32}a_{12} & a_{33}a_{13} & a_{12}a_{33} + a_{13}a_{32} & a_{13}a_{31} + a_{11}a_{33} & a_{11}a_{32} + a_{12}a_{31} \\ a_{11}a_{21} & a_{12}a_{22} & a_{13}a_{23} & a_{12}a_{23} + a_{13}a_{22} & a_{13}a_{21} + a_{11}a_{23} & a_{11}a_{22} + a_{12}a_{21} \end{bmatrix}$$

A.15.

Similarly, the transformation law for the strain in its abbreviated notion is

$$\varepsilon_I' = N_{IJ} \varepsilon_J \qquad \text{A.16.}$$

where the transformation matrix [N] is

$$[N]=\begin{bmatrix} a_{11}^2 & a_{12}^2 & a_{13}^2 & a_{12}a_{13} & a_{13}a_{11} & a_{11}a_{12} \\ a_{21}^2 & a_{22}^2 & a_{23}^2 & a_{22}a_{23} & a_{23}a_{21} & a_{21}a_{22} \\ a_{31}^2 & a_{32}^2 & a_{33}^2 & a_{32}a_{33} & a_{33}a_{31} & a_{31}a_{32} \\ 2a_{21}a_{31} & 2a_{22}a_{32} & 2a_{23}a_{33} & a_{22}a_{33}+a_{23}a_{32} & a_{21}a_{33}+a_{23}a_{31} & a_{22}a_{31}+a_{21}a_{32} \\ 2a_{31}a_{11} & 2a_{32}a_{12} & 2a_{33}a_{13} & a_{12}a_{33}+a_{13}a_{32} & a_{13}a_{31}+a_{11}a_{33} & a_{11}a_{32}+a_{12}a_{31} \\ 2a_{11}a_{21} & 2a_{12}a_{22} & 2a_{13}a_{23} & a_{12}a_{23}+a_{13}a_{22} & a_{13}a_{21}+a_{11}a_{23} & a_{11}a_{22}+a_{12}a_{21} \end{bmatrix}$$

A.17.

Transformation of C_{IJ} can be obtained by applying Equation A.14 to Hooke's Law (Equation A.12).

$$[\sigma']=[M][C][\varepsilon] \qquad \text{A.18.}$$

The inverse of Equation A.16 is

$$[\varepsilon]=[N]^{-1}[\varepsilon'] \qquad \text{A.19.}$$

Substitution for [ε] in Equation A.19 gives

$$[\sigma']=[M][C][N]^{-1}[\varepsilon'] \qquad \text{A.20.}$$

Comparison of Equation A.20 with Hooke's Law (Equation A. 1) shows

$$[C']=[M][C][N]^{-1} \qquad \text{A.21.}$$

Investigation of the two transformation matrixes [M] and [N] in Equation A. 15 and A.17 gives

$$[N]^{-1}=[M']$$

Therefore the transformation law for elastic constants C_{IJ} is

$$[C']=[M][C][M']$$

or

$$C'_{kl}=M_{ki}M_{lj}\,C_{ij} \qquad \text{A.22.}$$

In a similar manner, the transformation law for compliance is

$$S'_{kl} = N_{ki} N_{lj} S_{ij} \qquad \text{A.23.}$$

The primary advantage of Equations A.22 and A. 23 is that they can be applied directly to elastic constants given in abbreviated subscript notation. They are economical of space and easy to manipulate compared to the awkward work required to the full subscript notation. The derivation demonstrated above strictly follows the general tensor transformation. Therefore, results in Equations A.22 and A. 23 indicate that the abbreviated subscript notation C_{IJ} and S_{IJ} are indeed second order six-dimensional tensors, rather than the matrix notion only. Thus, all tensor properties do apply to them.

BIOGRAPHY OF THE AUTHOR

Miao Sun was born and raised in Shenyang city, a northeast city in P. R of China. She finished her college in University of Shanghai for Science & Technology in 1989 with a Bachelor's degree in Mechanical Engineering. She came to United State in 2000 and entered the Mechanical Engineering graduate program at the University of Maine in the fall of 2000.

After receiving her degree, she will be joining Department of Engineering Science and Mechanics at The Virginia Tech (Virginia Polytechnic Institute and State University) for a Ph, D. program. Miao is a candidate for the Master of Science degree in Mechanical Engineering from The University of Maine in August, 2002.